(2)

A CONTINUUM APPROACH TOWARD MODELING THE MECHANICS OF SOLID LUBRICATING FILMS

Final Report for Period March - September 1990

Jed A. Walowit, Inc.
4 Cypress Point
Clifton Park, New York 12065

Under contract to

Office of Naval Research

Arlington, Virginia

Contract No. N00014-90-C-0087

Approved for public release; distribution unlimited

September 1990

REPORT DOCUMENTATION PAGE

Form Approved
OMB No. 0704-0188

1a. REPORT SECURITY CLASSIFICATION Unclassified	1b. RESTRICTIVE MARKINGS None
2a. SECURITY CLASSIFICATION AUTHORITY	3. DISTRIBUTION/AVAILABILITY OF REPORT Approved for public release; distribution unlimited
2b. DECLASSIFICATION/DOWNGRADING SCHEDULE	
4. PERFORMING ORGANIZATION REPORT NUMBER(S) JAW-90-TR-1	5. MONITORING ORGANIZATION REPORT NUMBER(S)
6a. NAME OF PERFORMING ORGANIZATION Jed A. Walowit, Inc 6b. OFFICE SYMBOL (If applicable)	7a. NAME OF MONITORING ORGANIZATION
6c. ADDRESS (City, State, and ZIP Code) 4 Cypress Point Clifton Park, NY 12065	7b. ADDRESS (City, State, and ZIP Code)
8a. NAME OF FUNDING/SPONSORING ORGANIZATION Office of Naval Research 8b. OFFICE SYMBOL (If applicable)	9. PROCUREMENT INSTRUMENT IDENTIFICATION NUMBER N00014-90-C-0087
8c. ADDRESS (City, State, and ZIP Code) 800 N. Quincy Street Arlington, VA 22217	10. SOURCE OF FUNDING NUMBERS PROGRAM ELEMENT NO. / PROJECT NO. / TASK NO. / WORK UNIT ACCESSION NO.

11. TITLE (Include Security Classification)
A Continuum Approach Toward Modeling the Mechanics of Solid Lubricating Films (U)

12. PERSONAL AUTHOR(S)
Walowit, Jed A.

13a. TYPE OF REPORT	13b. TIME COVERED	14. DATE OF REPORT (Year, Month, Day)	15. PAGE COUNT
Final	FROM MAR90 TO SEP90	90SEP21	55

16. SUPPLEMENTARY NOTATION

17. COSATI CODES			18. SUBJECT TERMS (Continue on reverse if necessary and identify by block number)		
FIELD	GROUP	SUB-GROUP	Solid Lubricant	Plastic	Thermal
			Film	Elastic	Rheology
			Friction	Viscous	

19. ABSTRACT (Continue on reverse if necessary and identify by block number)

Analyses are developed to predict the tractive forces that will occur in a rolling-sliding contact between one body of a single material and a second body containing a thin coating of solid lubricant. Isotropic materials and conditions of plane strain are assumed. The loaded coating thickness is taken to be large compared with asperity heights but small compared with contact dimensions. The contact pressures are assumed to be high compared with the shear yield stress of the coating which in turn is taken to be small compared with those of the substrates.

An initial analysis is presented for approximating tractions under conditions of low slide to roll ratios which includes elastic, plastic, creep and thermal interactions. This analysis implements an approach developed for elastohydrodynamic lubrication at pressures and

(continued next page)

20. DISTRIBUTION/AVAILABILITY OF ABSTRACT	21. ABSTRACT SECURITY CLASSIFICATION
☐ UNCLASSIFIED/UNLIMITED ☐ SAME AS RPT. ☐ DTIC USERS	Unclassified
22a. NAME OF RESPONSIBLE INDIVIDUAL	22b. TELEPHONE (Include Area Code) / 22c. OFFICE SYMBOL

Block 19. (continued)

shear rates where the lubricant exhibits solid-like behavior but is oriented toward solid lubrication and includes a more extensive thermal analysis. Solutions are presented which show the influence of elastic modulus, rheological model, yield stress and pressure and temperature dependence of mechanical properties on predicted traction and shear stress behavior.

An analysis is presented which reduces the Levy-Von Mises equations for a plastic-rigid system so as to approximate thin film behavior under conditions of high slip rate. This analysis shows the expected development of a nearly hydrostatic state of stress for the coating in the contact zone but also shows that the film cannot support a pressure gradient when yielding occurs inside the coating. In particular it shows that the Hertzian pressure distribution required to sustain a constant film thickness cannot be maintained when the shear stress inside the coating reaches the shear yield stress over a significant portion of the contact zone.

An example is provided for the motion of a visco-plastic coating on a rigid substrate in contact with a rigid, linearly inclined slider. It is shown that for any given slider inclination, minimum film thickness and mechanical properties of the coating, a critical speed exists that when exceeded results in a complete loss of load capacity. Although this does not imply failure of the lubricant, it does further demonstrate the conclusion that traction and film formation cannot be treated separately at high slip rates.

FORWARD

This research was sponsored by the Office of Naval Research under ONR Contract Number N00014-90-C-0087. The Scientific Officer was Dr. Peter Schmidt. The author wishes to acknowledge Mr. Marshall B. Peterson of ONR/NIST who provided supervision and guidance, Dr. Pradeep K. Gupta for helpful discussions at the start of the program and Dr. Hooshang Heshmat of Mechanical Technology Incorporated for his valuable suggestions throughout the course of the program.

TABLE OF CONTENTS

LIST OF FIGURES

NOMENCLATURE

a	characteristic length, half width of contact zone or length of slider
c_i	specific heat of region i
D	Deborah number, $\mu_0 u_r/(Ga)$
d	surface displacement
$\hat{d}$	dimensionless surface displacement, $2rd/a^2$
E	elastic modulus
$\bar{e}$	effective strain rate, see Equation (20)
F	derivative function, $d\tilde{\tau}'/d\xi$
f	frictional force per unit transverse length
$\hat{f}$	dimensionless frictional force, $f/(ak)$
G	shear modulus
h	coating thickness
h^*	constant related to flow, $2Q/(u_0 h)$
$\hat{h}^*$	dimensionless constant, h^*/h^0
h_0	characteristic coating thickness, minimum coating thickness under linear slider
h_1	maximum coating thickness under linear slider
$\hat{h}_1$	dimensionless coating thickness, h_1/h_0
K_i	thermal conductivity of region i
k	shear yield stress
$\hat{k}$	dimensionless stress, k/k_0
k_0	characteristic value of shear yield stress
p	pressure
$\tilde{p}$	dimensionless pressure, p/p_0
$\hat{p}$	dimensionless pressure, $ph_0/(ak)$
p_h	maximum Hertz pressure
p_0	reference pressure, taken as p_h for Hertz contact
Q	volumetric flow per unit transverse length
q_1, q_2	heat flux crossing surface of region 1,2
$\tilde{q}_1$	dimensionless heat flux, $q_1/(\psi u_r s \tau_{c0})$
P_i	Peclet number for region i, $u_i a/\kappa_i$
R_i	volumetric rate of heat generation for region i
r	cylinder radius
s	slide to roll ratio, $\Delta u/u_r$
S	dimensionless shear rate parameter, $\mu_0 u_r s/(h\tau_{c0})$

t_r	residence time in contact zone
T	temperature
$\tilde{T}$	dimensionless temperature rise, $(T - T_0)/T_r$
T_0	surface temperature at start of contact
T_r	reference temperature rise, $u_r sa\psi\tau_{c0}/K_1$
u	velocity in x direction
$\hat{u}$	dimensionless velocity, u/u_0
u_r	rolling speed
u_0	characteristic velocity in x direction
u_1, u_2	speed of region 1,2
v	velocity in y direction
$\hat{v}$	dimensionless velocity, $va/(h_0 u_0)$
W	load per unit transverse length
$\hat{W}$	dimensionless load, $Wh_0/(a^2 k)$
x	coordinate in along surface
y	coordinate perpendicular to surface
α	viscosity - pressure coefficient
$\tilde{\alpha}$	dimensionless coefficient, αp_h
β	limiting shear stress - pressure coefficient
$\tilde{\beta}$	dimensionless coefficient, βp_h
γ	viscosity - temperature coefficient
$\tilde{\gamma}$	dimensionless coefficient, γT_r
Δh	inclination of slider, $h_1 - h_0$
ΔT_1^*	temperature rise on surface 1 at center of contact for uniform flux
ΔT_3	temperature rise in coating
Δu	slip rate, $u_1 - u_2$
Δu_h	slip velocity at $y = h$
Δu_0	slip velocity at $y = 0$
δ	dimensionless parameter, $(h_0/a)(k_0/p_0)$
δ^*	dimensionless parameter, maximum of δ and $(a/h_0)^2$
$\dot{\epsilon}$	shear rate
η	dimensionless coordinate, y/a
κ_i	thermal diffusivity for region i
λ	limiting shear stress - temperature coefficient
$\tilde{\lambda}$	dimensionless coefficient, λT_r
μ	viscosity
μ_0	viscosity at ambient pressure and temperature T_0

$\tilde{\mu}$ dimensionless viscosity, μ/μ_0

$\hat{\mu}$ dimensionless viscosity-speed parameter, $\mu u_0/(h_0 k)$

$\hat{\mu}^*$ critical value of $\hat{\mu}$ beyond which $\hat{W} = 0$

ν Poisson's ratio

ξ dimensionless coordinate, x/a

ρ_i density of region i

$\tilde{\sigma}$ effective stress, see Equation (19)

σ_x, σ_y coordinate stresses in x,y directions

$\hat{\sigma}_x, \hat{\sigma}_y$ dimensionless coordinate stresses, σ_x/p_0, σ_y/p_0

σ_z dimensionless stress in transverse direction

τ shear stress

$\hat{\tau}$ dimensionless shear stress, τ/k

$\tilde{\tau}$ dimensionless shear stress, τ/τ_{c0}

$\bar{\tau}$ average shear stress in contact zone

$\bar{\tilde{\tau}}$ dimensionless average shear stress, $\bar{\tau}/\tau_{c0}$

τ' shear stress without regard to limiting shear stress

$\tilde{\tau}'$ dimensionless shear stress, τ'/τ_{c0}

$\dot{\tau}'$ time derivative of τ'

τ_c characteristic shear stress function used in rheological model

$\tilde{\tau}_c$ dimensionless shear stress, τ_c/τ_{c0}

τ_{c0} characteristic shear stress at ambient pressure and temperature T_0

τ_m limiting shear stress

$\tilde{\tau}_m$ dimensionless limiting shear stress, τ_m/τ_{c0}

τ_h shear stress at y = h

$\hat{\tau}_h$ dimensionless shear stress, $-\tau_h/k$

τ_0 shear stress at y = 0

$\hat{\tau}_0$ dimensionless shear stress, $-\tau_0/k$

$\hat{\tau}_{max}$ maximum of $\hat{\tau}_0$ and $\hat{\tau}_h$

ϕ function characterizing rate dependence in rheological model

χ limiting shear stress ratio, τ_m/τ_c, presently taken near 1

ψ flux partition fraction, see Equation (11)

Subscripts

1 upper region (see Figure 1)

2 lower region (see Figure 1)

3 coating

i region variable, i = 1,2,3

j particular point in discretized ξ grid, used in finite difference solution

I. INTRODUCTION

Solid lubricants have been in use for many years in situations where extreme temperature, pressure or environmental conditions prohibit the use of liquid lubricants. Present requirements for high temperature and hostile environment applications create an increasing need for improved solid lubrication. Although considerable strides have been made in the development and implementation of solid lubricants, they have been somewhat hampered by a lack of quantitative methods for assessing the performance of solid films.

This study is intended to represent a step towards the objective of developing a tractable means for predicting the performance of solid lubricating films in machinery based upon property data obtained under laboratory conditions. Performance characteristics under consideration include surface and sub-surface temperature, friction, operating coating thickness and wear rates. These quantities may in turn be used to establish the useful life and applicability of a solid lubricant for a given application.

Considerable emphasis is placed here on the need for a tractable approach. Although an ultimate goal of predicting performance of solid lubricants based upon molecular structure should be pursued, a shorter term approach is also necessary to satisfy current needs even though it might require additional property data. This approach involves treating the solid lubricant as a continuum and modeling the rheology of the contact based on properties of both the lubricant and its immediate surroundings.

This investigation deals with an idealized isotropic lubricant under conditions of plane strain. Normal stresses due to loading are assumed in general to be high compared with the shear yield stress of the lubricant. The film is assumed to be thick compared with asperity heights but thin compared with contact lengths. In the first part of the study, as described in the next section, the existence of such a film is assumed and efficient algorithms are generated for predicting tractions based on contact geometry, operating conditions and the rheological model for the lubricant. Rheological models include a linear elastic component, a non-linear rate dependent component and a limiting shear stress. Properties are allowed to be dependent on both temperature and pressure. A thermal analysis is included and coupling between the effects of heat generation and temperature dependent properties is treated. Numerical examples are presented which show the influence of the various parameters on shear stress behavior. The second part of the study, described in Section III, deals with the ability to form and sustain the films assumed above and limitations that occur when the slip rates are high and is intended to provide guidance regarding the range of validity of both the present and previous traction models.

II. INITIAL TRACTION ANALYSIS

A combined thermal-elastic-plastic-creep model is presented here for estimating tractive forces resulting from shearing of solid films. Models of this type have been used successfully in the past for predicting tractive forces arising in concentrated contacts with liquid lubricants. Under the extreme pressures characteristic of these contacts, liquids behave similarly to solids in that elastic properties become significant at low shear rates and plastic yielding occurs at higher shear rates.

It will be assumed that the film is thick compared with the surface asperities on the mating surface and the load is sufficiently high that the asperities are fully imbedded in the film. A nearly hydrostatic state of stress will be assumed to exist in the contact zone. The normal loading will affect the size of the contact zone for elastic substrates and the pressure distribution within the contact zone. It is assumed however, that the only dependence of shear forces on the normal loading arises from pressure dependence of mechanical properties.

Based on the above assumptions the initial traction model will be an adaptation of that used for elastohydrodynamic applications[1,2]. The extensions put forth here will include coupling with a fairly general thermal analysis and the ability to treat pressure distributions other that Hertzian.

The development of the traction model contained herein, will proceed with a formulation of the mechanical problem, a formulation of the thermal problem, a description of the method of solution to the combined problem followed by some parametric studies.

A. Formulation of Mechanical Problem

The analysis developed thus far is based on a two dimensional geometric model depicted in Figure 1. A rolling - sliding contact is depicted with surfaces moving at speeds u_1 and u_2. A contact zone is formed between $x = 0$ and $x = 2a$ where the coating thickness is assumed to have a constant value h. The shear stress τ acting on the upper surface, will be in the direction shown when $u_1 > u_2$. A class of rheological models in the form

$$\dot{e} = \frac{\dot{\tau}'}{G} + \frac{\tau_c}{\mu}\phi(\tau'/\tau_c) \quad , \tag{1}$$

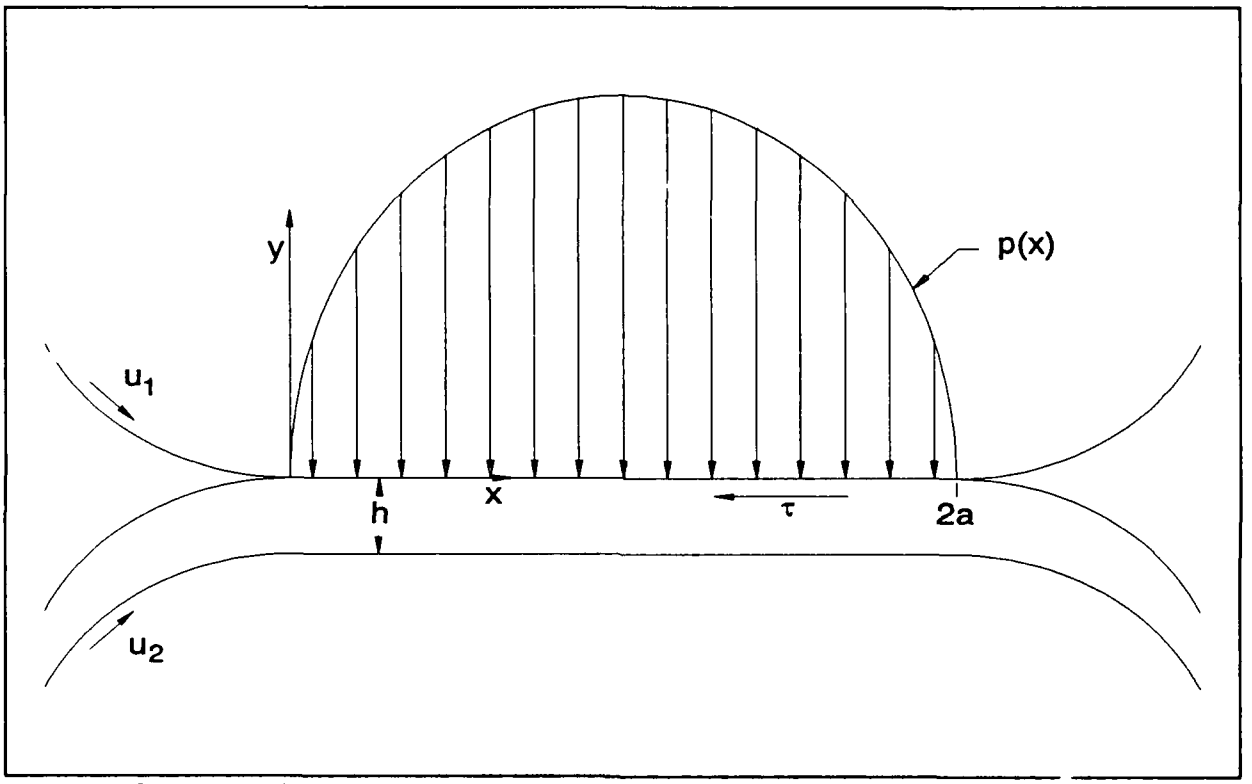

Figure 1. Schematic of geometry for traction analysis.

$$\tau = \min(\tau', \tau_m) = \begin{cases} \tau' & , \quad |\tau'| < \tau_m \\ \tau_m \tau'/|\tau'| & , \quad |\tau'| \geq \tau_m \end{cases} ,$$

will be examined. In the above equation **G** represents a shear modulus, τ_m is a maximum limiting shear stress, and τ_c and μ are constants and ϕ is a function describing the creep characteristics of the coating. If ϕ is chosen so that its limiting form at small values of its argument approaches its argument then μ would reduce to a viscosity at low shear stress. In general all of the properties in the above model can be dependent on temperature and pressure, however elastic properties will be somewhat less sensitive than creep and plastic properties and will be taken to be constant. This includes both the shear modulus of the coating, **G**, as well as the elastic properties of the substrate.

The variation of pressure across a thin film will be negligible. For thin metallic films the thermal conductivity will be sufficiently high so that the variation in temperature across the film will be small when compared with the variation along the film. If properties are taken to be constant across the film (evaluated at either the surface temperature, the centerline temperature or a mean temperature) then the velocity distribution will vary linearly across the film and the strain rate will be given by $\dot{e} = \Delta u/h$, where $\Delta u = u_1 - u_2$.

If the rolling speed $u_r = (u_1 + u_2)/2$ is large compared with the slip rate Δu, one may approximate the shear stress derivative with $\dot{\tau}' = u_r \, d\tau'/dx$ and the top part of Equation (1) may be written as

$$\frac{\Delta u}{h} = \frac{u_r}{G}\frac{d\tau'}{dx} + \frac{\tau_c}{\mu}\phi(\tau'/\tau_c) \quad . \tag{2}$$

The pressure and temperature dependence of properties τ_c, τ_m, and μ may be expressed as

$$\tau_c = \tau_{c0}\,\tilde{\tau}_c(\tilde{p},\tilde{T}) , \qquad \tau_m = \tau_{m0}\,\tilde{\tau}_m(\tilde{p},\tilde{T}) , \qquad \mu = \mu_0\,\tilde{\mu}(\tilde{p},\tilde{T}) ,$$

where τ_{c0}, τ_{m0}, and μ_0 denote properties evaluated at the upstream surface temperature, T_0, and ambient pressure. The quantities $\tilde{p}$ and $\tilde{T}$ are dimensionless forms of the pressure **p**, and temperature **T**, scaled on suitable reference quantities which will be selected later.

One may now introduce the dimensionless variables and parameters

$$\tilde{\tau} = \frac{\tau}{\tau_{c0}} , \quad \xi = \frac{x}{a} , \quad \eta = \frac{y}{a} , \quad D = \frac{\mu_0 u_r}{Ga} , \quad s = \frac{\Delta u}{u_r} , \quad S = \frac{\mu_0 u_r}{h\tau_{c0}} s \tag{3}$$

to put Equation (1) in the dimensionless form

$$D\frac{d\tilde{\tau}'}{d\xi} = S - \frac{\tilde{\tau}_c}{\tilde{\mu}}\phi(\tilde{\tau}'/\tilde{\tau}_c)$$
$$\tilde{\tau} = \min(\tilde{\tau}', \tilde{\tau}_m) \ . \qquad (4)$$

If we neglect shearing effects in the inlet ($\xi < 0$) then the boundary condition on Equation (4) is

$$\tilde{\tau} = 0 \quad @ \ \xi = 0 \ . \qquad (5)$$

If properties were independent of pressure and temperature, or if the pressure and temperature were known as functions of position then Equations (4) and (5) could be solved for any prescribed function ϕ. Two particular functions to be considered initially are $\phi(\zeta) = \tanh^{-1}(\zeta)$ (to be referred to as the arctan model), which was used by Bair and Winer to characterize traction fluids and $\phi(\zeta) = \zeta$, the Maxwell model which has been used extensively in the analysis of viscoelastic behavior of materials.

The following representations will be implemented to characterize effects of property variations with temperature and pressure:

$$\mu = \mu_0 e^{\alpha p - \gamma(T - T_0)} \ , \quad \tau_c = \tau_{c0}\frac{1 + \beta p}{1 + \lambda(T - T_0)} \ , \quad \tau_m = \chi\tau_c \ . \qquad (6)$$

In order to couple Equation (6) with Equation (4) the relationships must be provided for determining the pressure **p**, and the temperature **T**, as functions of position **x**. Two types of pressure distributions that should be considered are a uniform distribution (whose relevance will be discussed in Section III) and an elliptical distribution corresponding to a Hertzian contact based on elastic properties of the substrate. This latter distribution which is illustrated in Figure 1 will be used in the initial analysis. Thus

$$p = p_h\sqrt{1 - (\xi - 1)^2} \ , \qquad (7)$$

where p_h is the maximum Hertz pressure easily determined from the Hertz formulas for line contact along with the half width of the contact, **a**. The use of this relationship will be valid when $a/h >> 1$ and the

stiffness of the film in the contact zone is high compared those for the substrates.

B. Formulation of Thermal Problem

The amount to heat dissipated in the contact will depend on the shear stress distribution, hence the temperature distribution cannot be prescribed apriori. A form of the energy equation must therefore be coupled with the rheological equations given above. The energy equation will first be simplified based on high Peclet number approximations.

Since body 1 moves at a speed u_1, the residence time, t_r, of a point on its surface in the contact zone ($0 < x < 2a$) would be $t_r = 2a/u_1$. If the thermal diffusivity of body 1 is κ_1, then the thermal diffusion depth into body 1 would be $\sqrt{\kappa_1 t_r}$ and the ratio of the length of the contact zone, $2a$, to the diffusion depth would be $\sqrt{2P_1}$, where $P_1 = u_1 a/\kappa_1$ is the Peclet number for substrate 1. At high Peclet numbers the aspect ratio for conduction is large and conduction in the x direction becomes negligible compared with that in the y direction. Heat is thus transferred into the body by conduction and carried away by its motion. The same argument can be applied to body 2 if it is moving rapidly. The coating, designated as region 3, will have a high aspect ratio since it is assumed throughout the analysis that $a/h >> 1$. The energy equation for region i may then be written as:

$$\rho_i c_i u_i \frac{\partial T}{\partial x} = K_i \frac{\partial^2 T}{\partial y^2} + R_i , \qquad i = 1,2,3 \quad . \tag{8}$$

The heat generation rates per unit volume R_i will be 0 for the elastic substrates and will be the product of the shear stress and the inelastic portion of the shear rate for the coating. Thus from Equations (1) and (2) the heat generation rate in the film is

$$R_3 = \begin{cases} \dfrac{\tau_c}{\mu}\tau' \phi\left(\dfrac{\tau'}{\tau_c}\right) , & \tau' < \tau_m \\ \tau_m \dfrac{\Delta u}{h} , & \tau' \geq \tau_m \end{cases} \quad . \tag{9}$$

Continuity of flux implies continuity of $K_i \partial T/\partial y$ at $y = 0, -h$ for $0 < x < 2a$. The boundary conditions on the temperature, T, are

$$\lim_{|y|\to\infty} T - T_0 \quad \text{and} \quad T - T_0 \ @ \ x - 0 \quad . \tag{10}$$

Although Equations (8) - (10) can be solved in their present form, further simplification can be obtained when the thermal resistance of the coating is small compared with that of either of the substrates. An upper bound to the temperature rise from the surface to the center of the film, ΔT_3, may be obtained by neglecting the effects of the convective motion of the film. The temperature rise in the film thus corresponds to that due to conduction between two parallel plates for a material generating heat at a rate R_3 which is $\Delta T_3 = R_3 h^2/(8K_3)$. At any point x along the film, the heat flux going into region 1 is $q_1 = \psi R_3 h$, where ψ is the fraction of heat generated going into region 1. One may obtain an estimate of the surface temperature rise by assuming R_3 and hence q_1 to be independent of x. The thermal problem reduces to that for a semi-infinite body moving past a uniform heat flux starting at $x = 0$ whose solution (or that for the analogous time transient problem of a uniform flux applied to the surface of a stationary semi-infinite body at time $t = 0$) may be found in many heat transfer texts (ie. Carslaw and Jaeger[3]). If one divides ΔT_3 by the surface temperature rise at the center of contact ($x = 1$) obtained from the solution to the above problem, ΔT_1^*, the following result is obtained:

$$\frac{\Delta T_3}{\Delta T_1^*} = \frac{h}{a}\frac{K_1}{K_3}\frac{\sqrt{\pi P_1}}{8\eta} \quad .$$

Although the Peclet number, P_1, is large, h/a will be very small for thin films and the above temperature ratio will be small as long as the thermal conductivities of the film and the substrate are of the same order of magnitude. This is frequently true for solid films, especially metallic films but is generally not true for liquid lubricants which have much lower thermal conductivities. In the latter case temperature variations across the film can be significantly larger than surface temperature rises.

The above arguments provide the criteria for neglecting temperature rises in the film. Doing so, reduces the thermal problem from a three region to a one region problem and more importantly provides justification for property variations across the film. In the remainder of this analysis temperature rises across the film will be neglected but the ability to handle the three region thermal problem at a later time will be retained.

With the above approximations Equation (8) needs to be solved only in region 1, $R_1 = 0$, and the boundary condition at $y \to -\infty$ given in Equation (10) is replaced by the condition at $y = 0$ that $K_1 \partial T/\partial y = h\psi R_3$. By equating temperatures at $y = 0$ and $y = h$ and noting that $q_1 + q_2 = hR_3$, one may determine the flux partition fraction

$$\psi = \frac{K_1\sqrt{P_1}}{K_1\sqrt{P_1} + K_2\sqrt{P_2}} \quad . \tag{11}$$

One may now introduce the reference temperature $T_r = u_r sa\psi\tau_{c0}/K_1$ and the additional dimensionless variables and parameters

$$\tilde{T} = \frac{T - T_0}{T_r} \; , \quad \tilde{q}_1 = \frac{q_1}{\psi u_r s \tau_{c0}} \; , \quad \tilde{\alpha} = \alpha p_h \; , \quad \tilde{\beta} = \beta p_h \; , \quad \tilde{\gamma} = \gamma T_r \; , \quad \tilde{\lambda} = \lambda T_r \; . \tag{12}$$

The dimensionless energy equation for region 1 becomes

$$\frac{\partial \tilde{T}}{\partial \xi} = \frac{1}{P_1}\frac{\partial^2 \tilde{T}}{\partial \eta^2} \quad , \tag{13}$$

with the boundary conditions on $\tilde{T}(\xi,\eta)$

$$\lim_{\eta \to \infty} \tilde{T}(\xi,\eta) = \tilde{T}(0,\eta) = 0 \tag{14}$$

and the surface flux loading

$$\frac{\partial \tilde{T}}{\partial \eta} = \tilde{q}_1 = \begin{cases} \dfrac{1}{S}\dfrac{\tilde{\tau}_c}{\tilde{\mu}}\tilde{\tau}'\phi\left(\dfrac{\tilde{\tau}'}{\tilde{\tau}_c}\right) & , \quad \tilde{\tau}' < \tilde{\tau}_m \\ \tilde{\tau}_m & , \quad \tilde{\tau}' \geq \tilde{\tau}_m \end{cases} \qquad \eta = 0 \; , \quad 0 < \xi < 2 \; . \tag{15}$$

C. Solution to Combined Problem

Equations (13) to (15) provide a statement of the thermal problem and Equations (4) and (5) along with the prescribed function ϕ, represent the mechanical problem. They are coupled through the property variation relationships given in Equation (6) which may be expressed in dimensionless form as:

$$\tilde{\mu} = e^{\tilde{\alpha}\tilde{p} - \gamma\tilde{T}}, \quad \tilde{\tau}_c = \frac{1 + \tilde{\beta}\tilde{p}}{1 + \tilde{\lambda}\tilde{T}}, \quad \tilde{\tau}_m = \chi\tilde{\tau}_c \quad , \tag{16}$$

where $\tilde{p} = p/p_h$.

A direct iteration scheme is used to couple the thermal problem with the mechanical problem. Initially the mechanical problem is solved for isothermal conditions ($\tilde{T} = 0$). This provides an initial shear stress distribution $\tilde{\tau}$ and from Equation (15) an initial flux loading, $\tilde{q}_1(\xi)$. One may now solve the thermal problem for a new temperature distribution to evaluate temperature dependent properties from Equation (16) which are then used in the next iteration of the mechanical problem. Convergence is achieved when the traction, defined as integral of the shear stress across the contact zone, deviates by less than a prescribed tolerance between iterations.

At each iteration Equation (4) may be treated as a first order non-linear differential equation below the limiting shear stress and an algebraic equation above it. At low pressures the Deborah number, **D**, which multiplies the derivative, can become quite small and compared with the second term on the left side of Equation (4). When this occurs Equation (4) assumes a very "stiff" behavior and explicit numerical integration methods such as Runge-Kutta tend to become unstable. To avoid this problem, a semi-implicit algorithm was implemented that has been widely used for stiff systems (see Press, et al.[4]) and is described below.

Put the top part of Equation (4) in the form $d\tilde{\tau}'/d\xi = F(\xi,\tilde{\tau}')$, discretize the ξ interval of interest into a grid, denote the values of ξ and $\tilde{\tau}'$ at the jth point as ξ_j and $\tilde{\tau}'_j$, and use the average value of **F** to increment $\tilde{\tau}'$ from it value at ξ_j to that at ξ_{j+1} as follows:

$$\tilde{\tau}'_{j+1} = \tilde{\tau}'_j + \frac{\xi_{j+1} - \xi_j}{2}\left[F(\xi_{j+1},\tilde{\tau}'_{j+1}) + F(\xi_j,\tilde{\tau}'_j) \right] \quad .$$

If $F(\xi_{j+1},\tilde{\tau}'_{j+1})$ in the above equation is approximated by

$$F(\xi_{j+1},\tilde{\tau}'_{j+1}) = F(\xi_{j+1},\tilde{\tau}'_j) + (\tilde{\tau}'_{j+1} - \tilde{\tau}_j)\left.\frac{\partial F}{\partial \tilde{\tau}'}\right|_{\xi_{j+1},\tilde{\tau}'_j}$$

and the ensuing expression is solved for $\tilde{\tau}'_{j+1}$, the result is

$$\tilde{\tau}'_{j+1} = \tilde{\tau}'_j + \frac{F(\xi_{j+1},\tilde{\tau}'_j) + F(\xi_j,\tilde{\tau}'_j)}{\frac{2}{\xi_{j+1}-\xi_j} - \left.\frac{\partial F}{\partial \tilde{\tau}'}\right|_{\xi_{j+1},\tilde{\tau}'_j}} \quad .$$

The above procedure is generally stable, provides quadratic accuracy and has proven to be very effective for the problem at hand.

Although the surface temperature $\tilde{T}(\xi,0)$, that satisfies Equations (13) and (14), for any surface flux distribution $\tilde{q}_1(\xi)$, can be determined with the convolution integral[3]

$$\tilde{T}(\xi,0) = \frac{1}{\sqrt{\pi P_1}} \int_0^{\xi} \frac{\tilde{q}_1(\xi')}{\sqrt{\xi - \xi'}} d\xi' \quad ,$$

it was found more expedient to adapt an existing finite difference routine written by the author[5]. The computer time is approximately the same and the finite difference approach provides sub-surface temperatures without the need for further computation. In addition the finite difference solution is readily amenable for use in treating the three region problem discussed previously as well as handling more general thermal boundary conditions such as convection or radiation from the surfaces.

D. Parametric Studies

A number of parametric studies have been performed to show the influence of viscosity and shear modulus on the nature of the shear stress profiles and the traction vs. slip rate behavior. A base case has been selected which will be referred to as the low viscosity, low compliance case. Medium and high viscosity cases will correspond to a factor of 10 and 100 increase in viscosity respectively. Medium and high compliances will correspond to 10 and 100 fold decreases in shear modulus. Non dimensional parameters for the base case are $D = 3.2\times10^{-6}$, $S = 6.4\times10^{-3}$ s, $\tilde{\alpha} = 10$ and $\chi \sim 1$. The above parameters would correspond to the physical parameters $u_r = 1000$ in/sec, $h = 6\times10^{-5}$ in, $a = 6\times10^{-3}$ in, $\tau_{c0} = 6000$ psi, $G = 1.2\times10^{5}$ psi, $\mu_0 = 2.3\times10^{-6}$ reyns, $\alpha = 10^{-4}$ in^2/lb and $p_h = 10^5$ psi.

The variation of the average shear stress, $\bar{\tilde{\tau}}$, with the slide to roll ratio, s, is shown in Figures 2 - 4 at various compliances for low, medium and high viscosities respectively. (The average shear stress is defined as the total load divided by the total contact area and $\bar{\tilde{\tau}}$ may be converted to a friction coefficient by dividing it

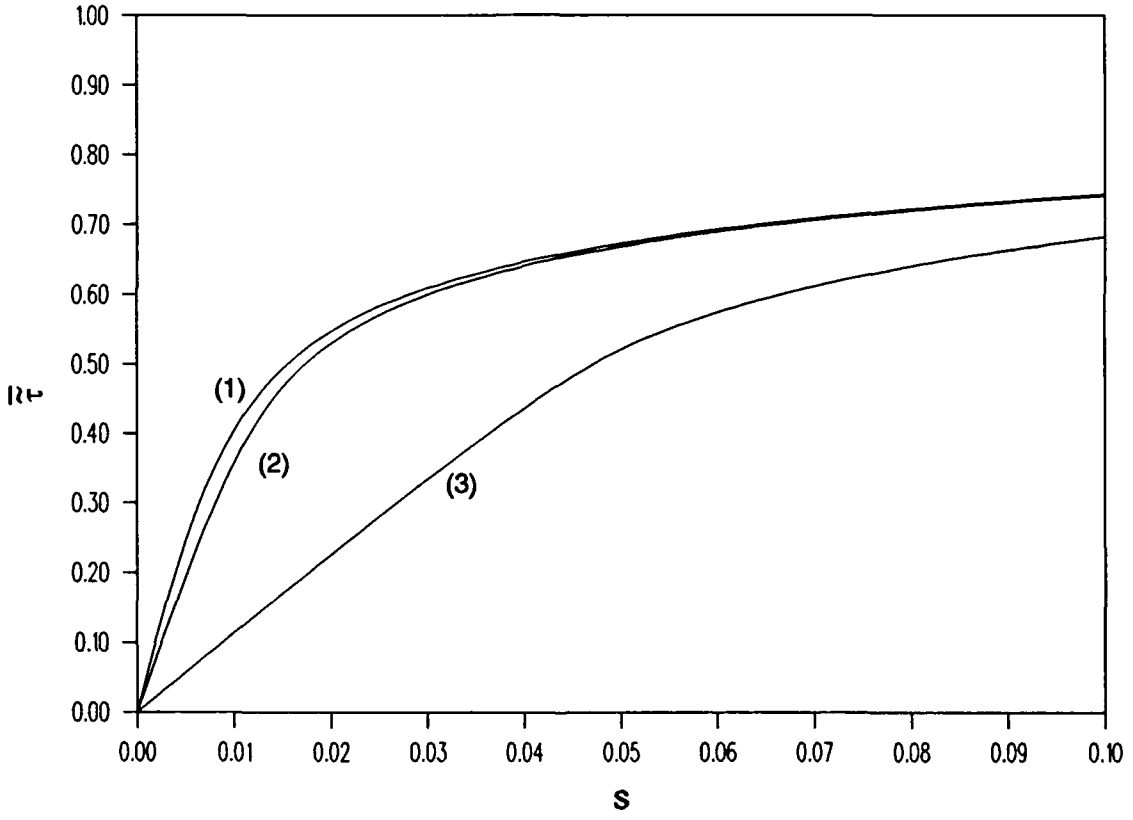

Figure 2. Traction vs. slip rate at low viscosity, arctan model, isothermal.

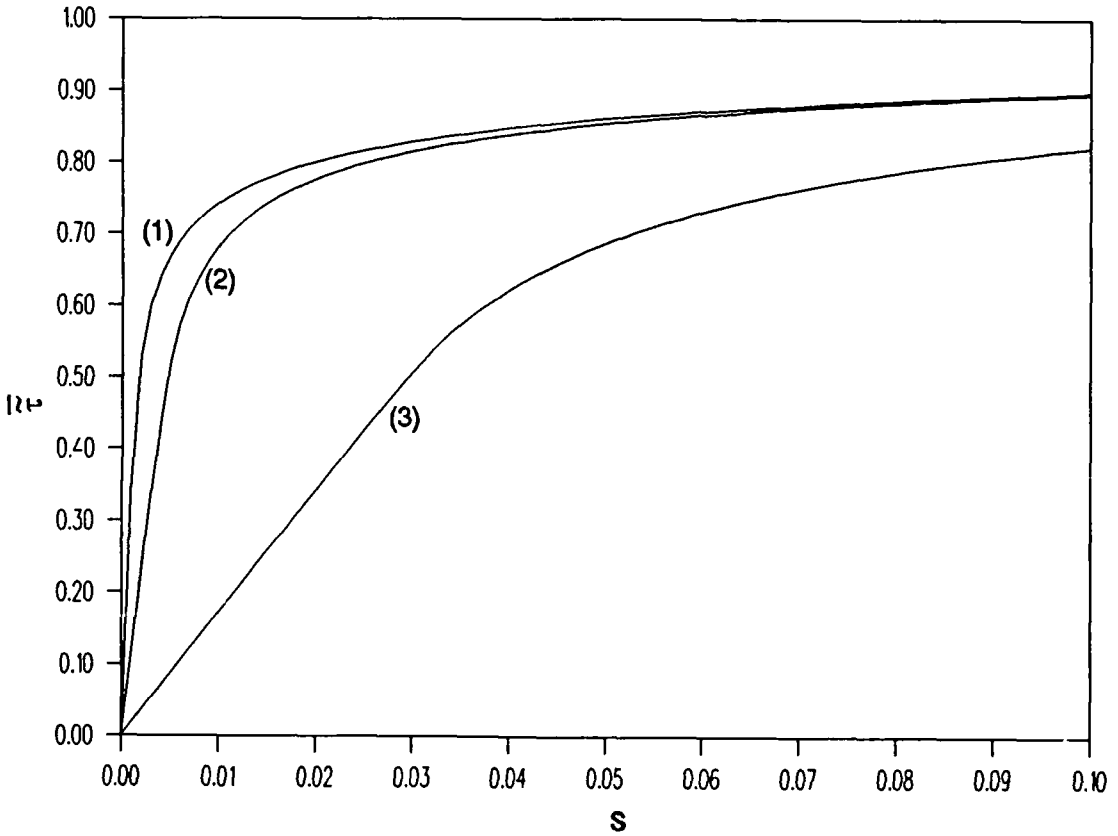

Figure 3. Traction vs. slip rate at medium viscosity, arctan model, isothermal.

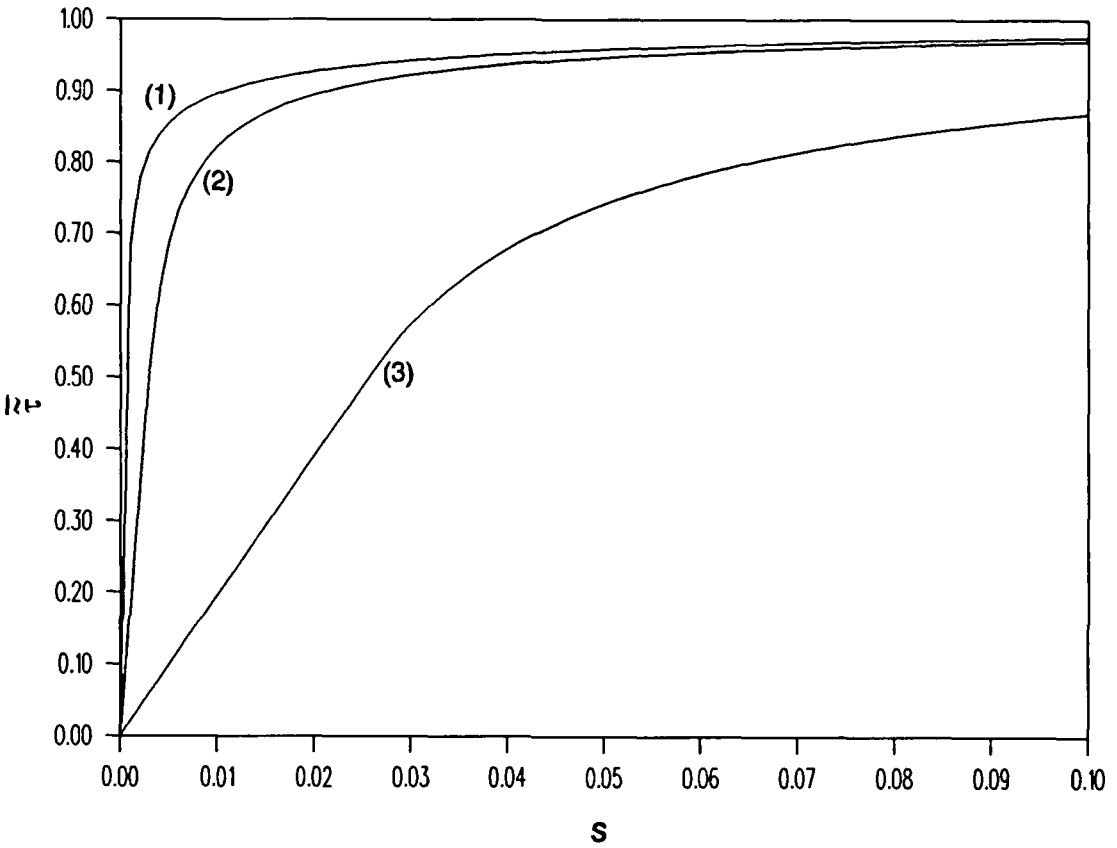

Figure 4. Traction vs. slip rate at high viscosity, arctan model, isothermal.

by $\pi p_h/(4\tau_{c0})$, which has a value of **13.1** for all of the numerical examples presented in this section.) The curves denoted by (1), (2) and (3) represent low, medium and high compliance respectively. These curves were obtained with the use of the arctan model without the inclusion of thermal effects. The arctan model provides an asymptotic approach to the limiting shear stress when $\chi = 1$. A value, of $\chi = .999$ was selected for use with the arctan model to provide a smooth transition but a definite cutoff point for the limiting shear stress.

Comparison of curves (1) and (2) in Figure 2 reveals that an order of magnitude drop in shear modulus produces very little change in predicted traction at low viscosity and the behavior is predominantly visco-plastic in nature. The behavior is somewhat different at high viscosity. Curves (1) and (2) in Figure 3 differ significantly at low slip rates but approach each other at higher slip rates where plastic behavior predominates. Curve (3) in Figure 4 lies fairly close to the corresponding curve in Figure 3 thus indicating predominantly elastic-plastic behavior where an order of magnitude change in viscosity has very little effect on traction. At high viscosity, low shear modulus and low slip rate, the behavior becomes primarily elastic with the dimensionless average shear stress, $\bar{\tilde{\tau}}$, approaching **S/D** corresponding to integration of Equation (4) with ϕ set equal to **0**.

In all of the curves described above the average shear stress increased with increasing slide to roll ratio. Inclusion of temperature dependent properties in some circumstances can actually show a decrease in traction due to a drop in the limiting shear stress and viscosity as the coating heats up. In order to include thermal effects, the additional parameters ψ, $\tilde{\gamma}$, $\tilde{\lambda}$ and P_1 must be prescribed. A value of $\psi = .5$ was selected for the thermal partition fraction as would be expected at low values of **s**, if the same material were used for both substrates. A value of $K_1 = 6$ lb-sec/°F corresponding approximately to the thermal conductivity of steel was selected which results in a reference temperature of $T_r = 3\times10^3\ s$ °F. Values of $\gamma = .00667$ and $\lambda = .0167$ were chosen which correspond to factor of two drops in viscosity and limiting shear stress at temperature rises of **100**°F and **60**°F respectively and result in dimensionless parameter values of $\tilde{\gamma} = 20s$ and $\tilde{\lambda} = 50s$. Finally a value of the Peclet number was chosen as $P_1 = 100$ for the base line case used in most of the parametric studies with a value of $P_1 = 500$ for the high Peclet number examples. The value for steel would lie approximately mid-way between these two cases. The effect of the Peclet number on the shear stress profiles is shown in Figure 5.

The variations of the average shear stress with slide to roll ratio analogous to Figures 2 - 4 but including thermal effects are shown in Figures 6 - 8. At low slip rates, thermal effects are small as can be seen by comparing the curves in Figures 6 - 8 with the corresponding curves in Figures 2 - 4. As the slip rate increases thermal effects cause the curves to level off more rapidly and in some cases tractions are seen

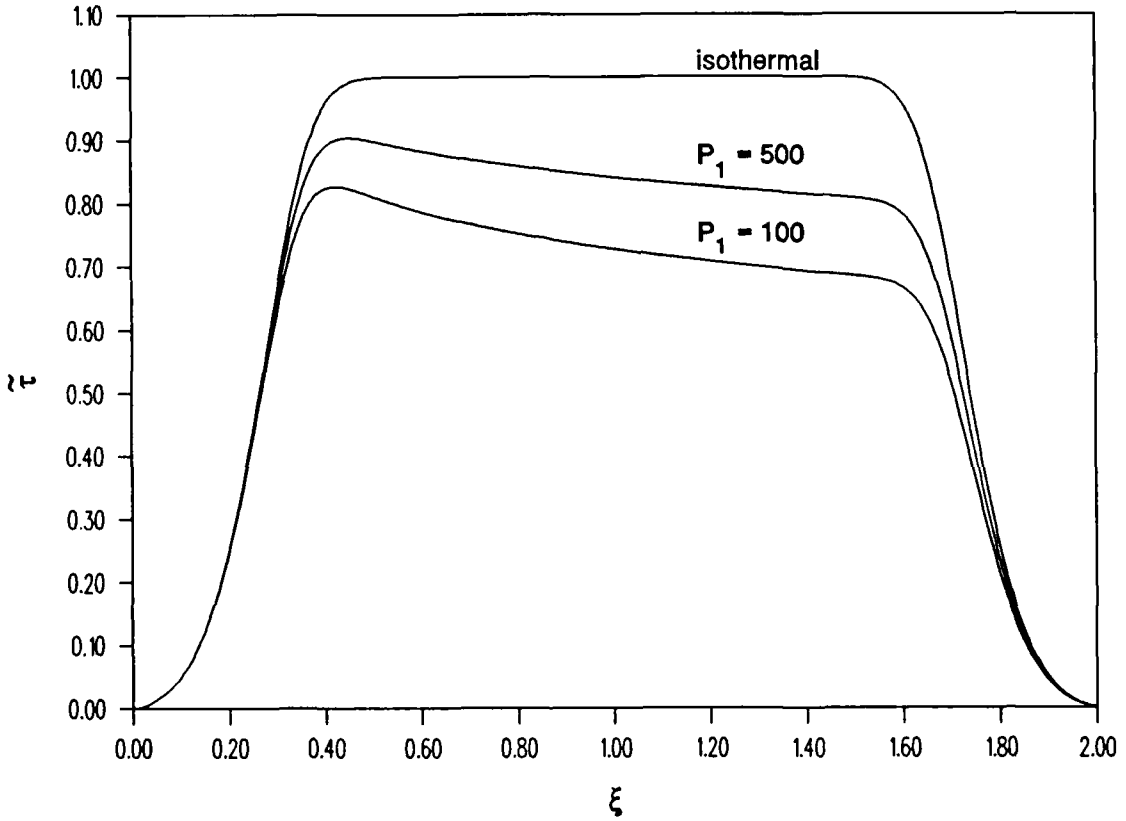

Figure 5. Effect of Peclet number on shear stress profile, low viscosity, low compliance, s = 0.1 .

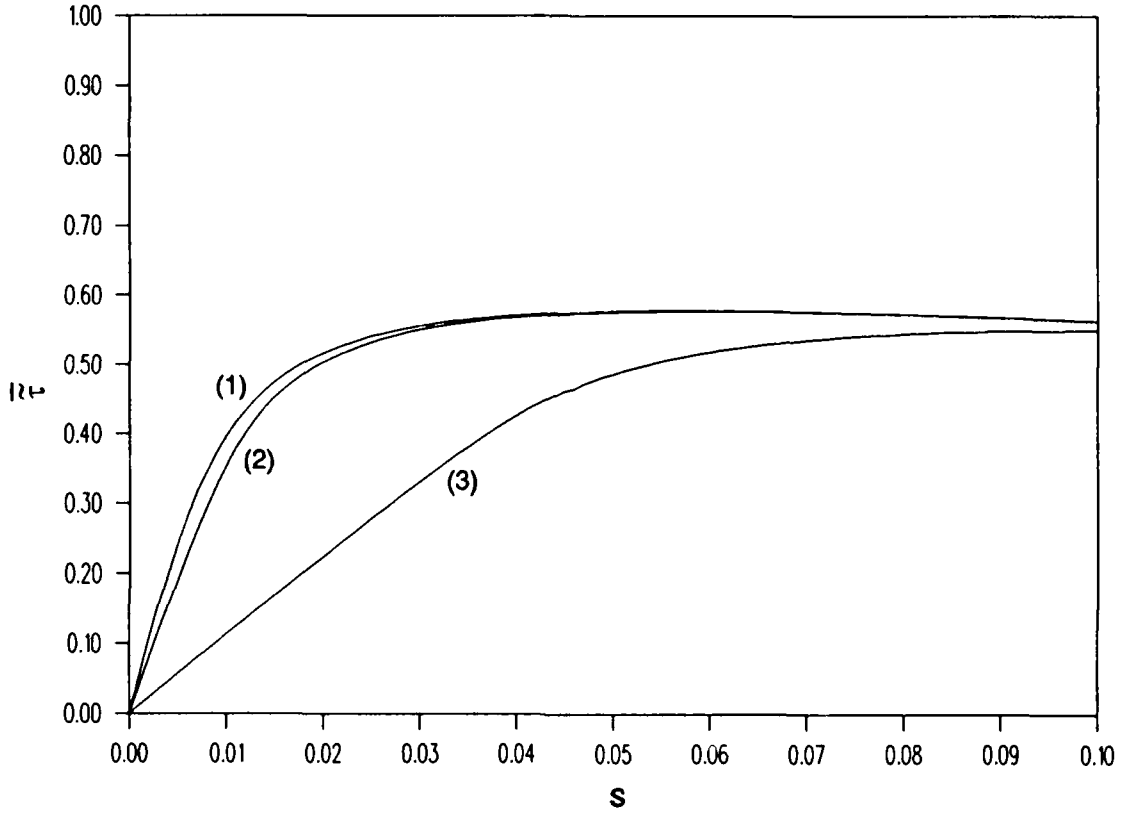

Figure 6. Traction vs. slip rate at low viscosity, arctan model with temperature dependent properties.

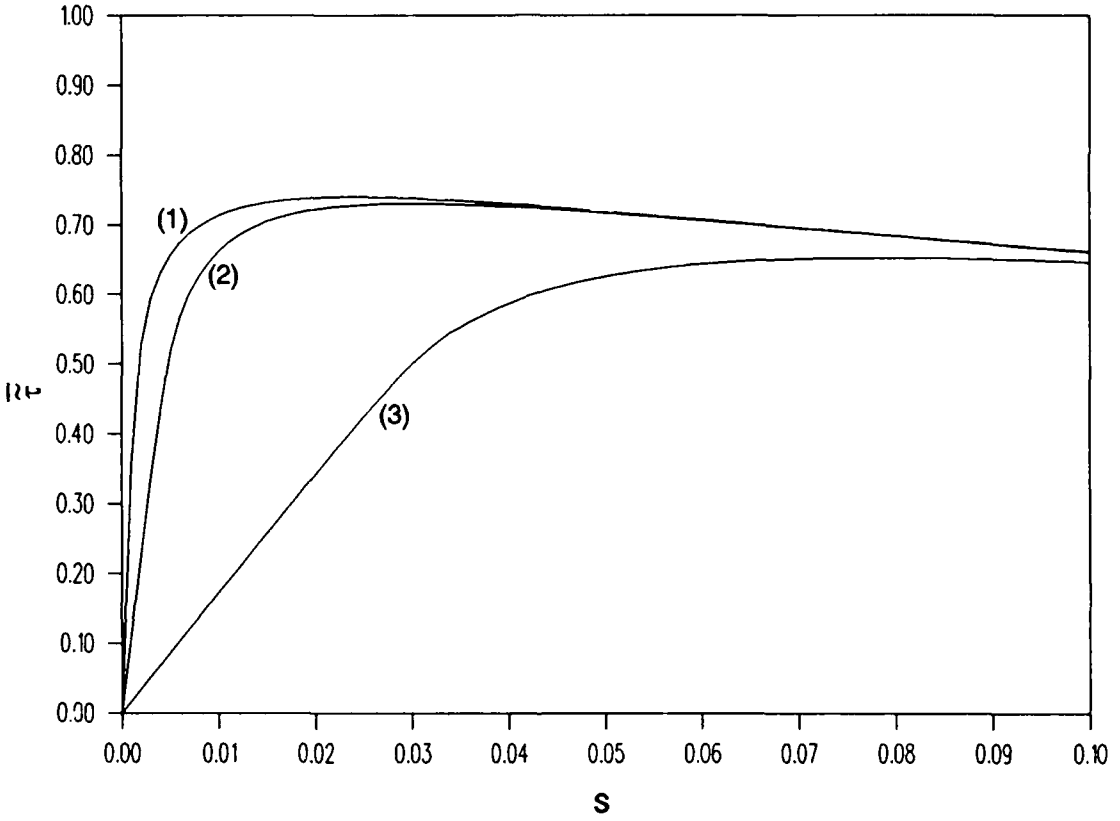

Figure 7. Traction vs. slip rate at medium viscosity, arctan model with temperature dependent properties.

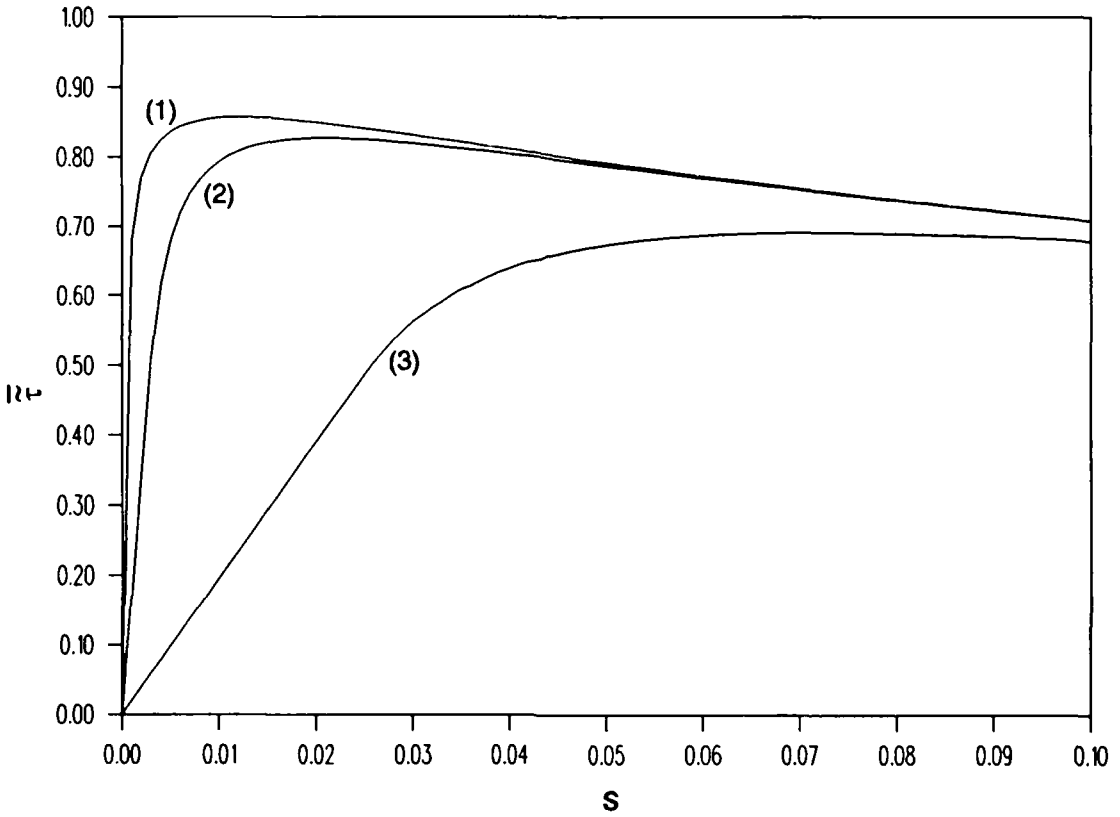

Figure 8. Traction vs. slip rate at high viscosity, arctan model with temperature dependent properties.

to decrease with increasing slip rates. At higher viscosities, thermal effects become visible at lower slip rates.

In order to investigate the sensitivity of the traction behavior to the rheological model, a series of parametric studies were carried out with the use of the Maxwell model. The same parameters were used for both models. Comparisons of the results obtained for the low and high viscosity cases with inclusion of thermal property variations are shown in Figure 9 and 10. The curves labelled (1-a) and (3-a) refer to the arctan model for the low and high compliance cases respectively. The corresponding curves for the Maxwell model are labelled (1-m) and (3-m). The Maxwell model, for the low viscosity case is seen to produce slightly higher tractions since the creep resistance does not level off with increasing shear rate as does the arctan model (see Figure 11). For the high viscosity case shown in Figure 10, however, the behavior is very nearly elastic-plastic and the traction curves for the two models become nearly indistinguishable.

The arctan model avoids the abrupt change in slope of the stress strain rate curve at the yield point characteristic of the Maxwell model. This abrupt change is not seen in the traction curves shown in Figures 9 and 10 because it is smoothed over by the integration process used in evaluating the average shear stress. It can be seen clearly, however, in the shear stress profiles shown in Figure 12. The upper two curves in the figure do not include the temperature variation in properties. In both cases the abrupt transition of the Maxwell model to the limiting shear stress is evident.

The corresponding dimensionless temperature profiles for the four curves in Figure 12 are shown in Figure 13. The upper curves were obtained by back calculating the temperature without including temperature variation in properties which corresponds to the first iteration performed in the process of obtaining the thermal solution. At the slip rate of $\mathbf{s} = .1$ used in obtaining Figures 12 and 13, a value of $\tilde{T}$ of **0.1** corresponds to a temperature rise of **30°F**.

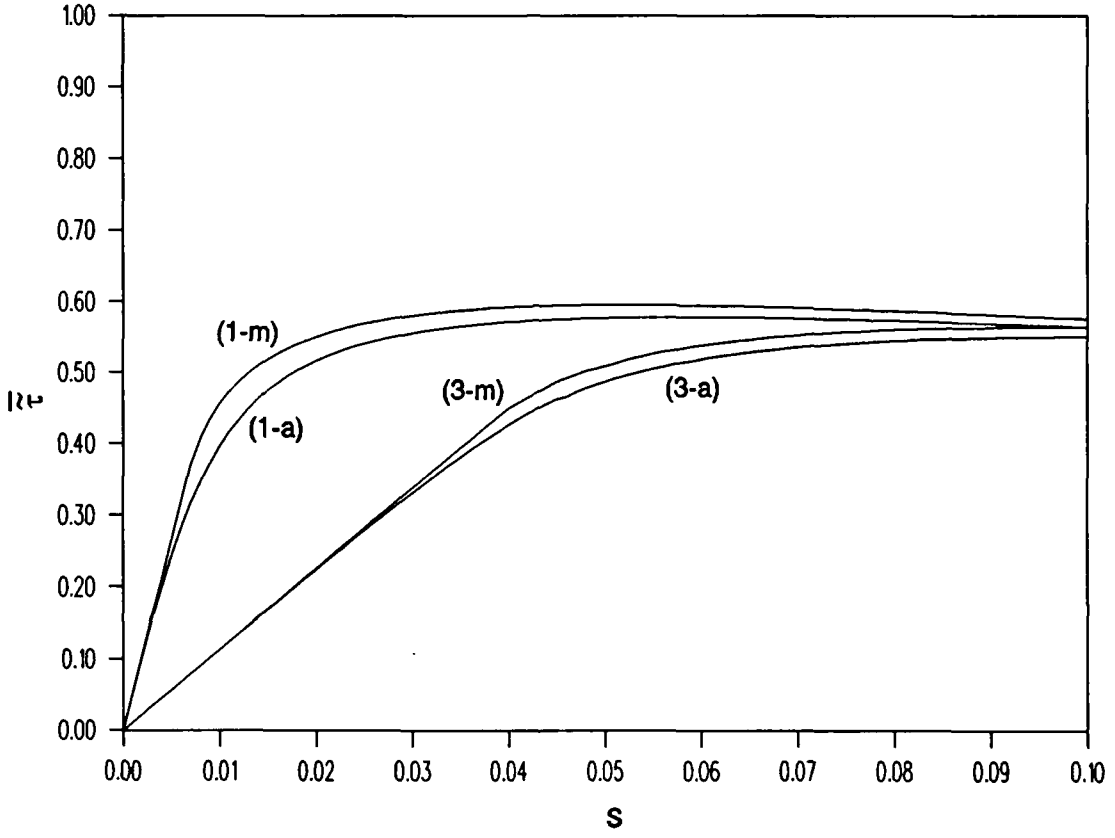

Figure 9. Comparison of traction vs. slip rate between arctan model and Maxwell model at low viscosity with temperature dependent properties.

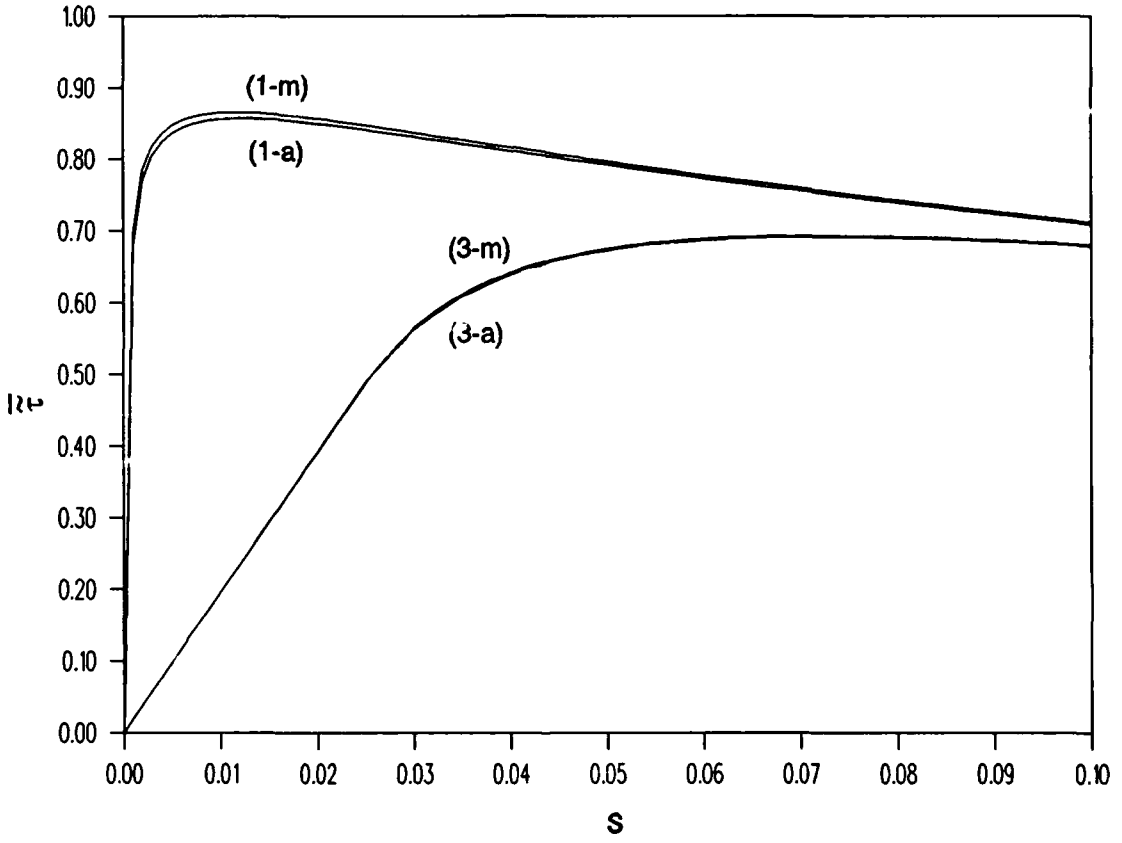

Figure 10. Comparison of traction vs. slip rate between arctan model and Maxwell model at high viscosity with temperature dependent properties.

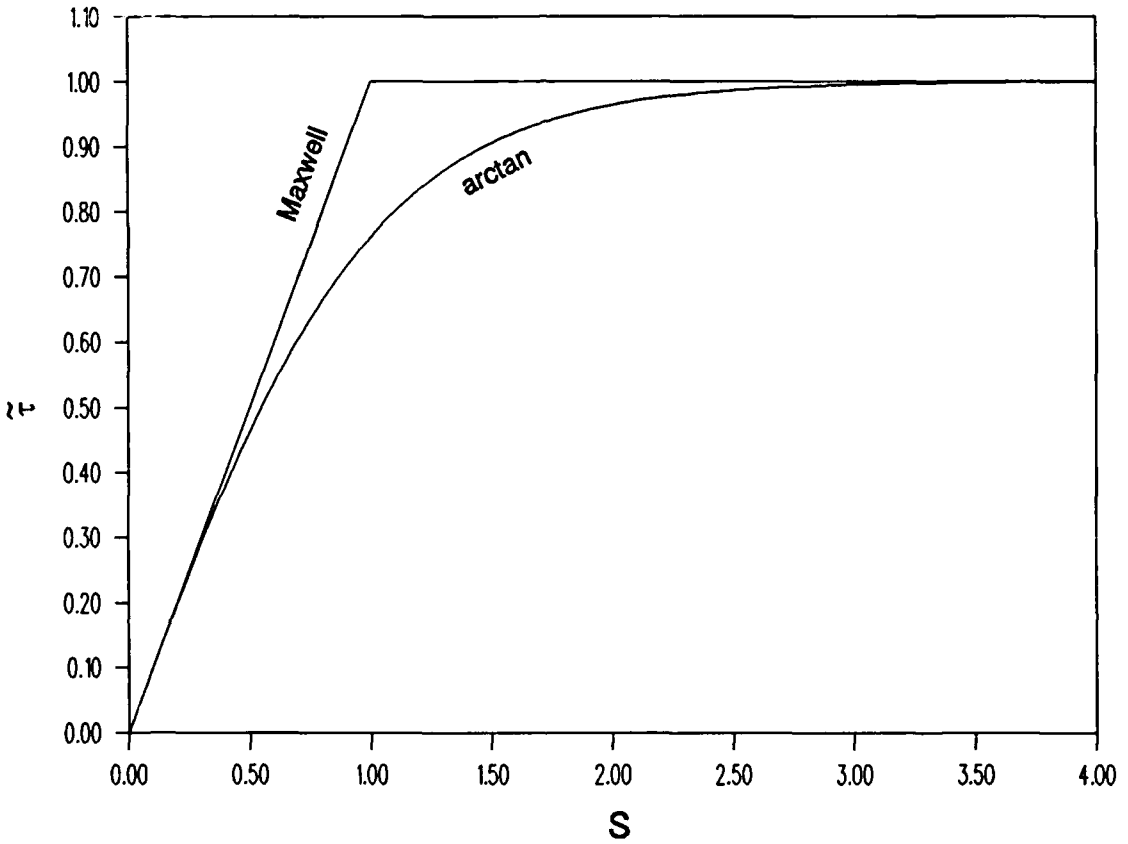

Figure 11. Comparison of dimensionless shear stress, $\tilde{\tau}$, vs. shear rate parameter, S, between arctan and Maxwell models under isothermal, inelastic conditions.

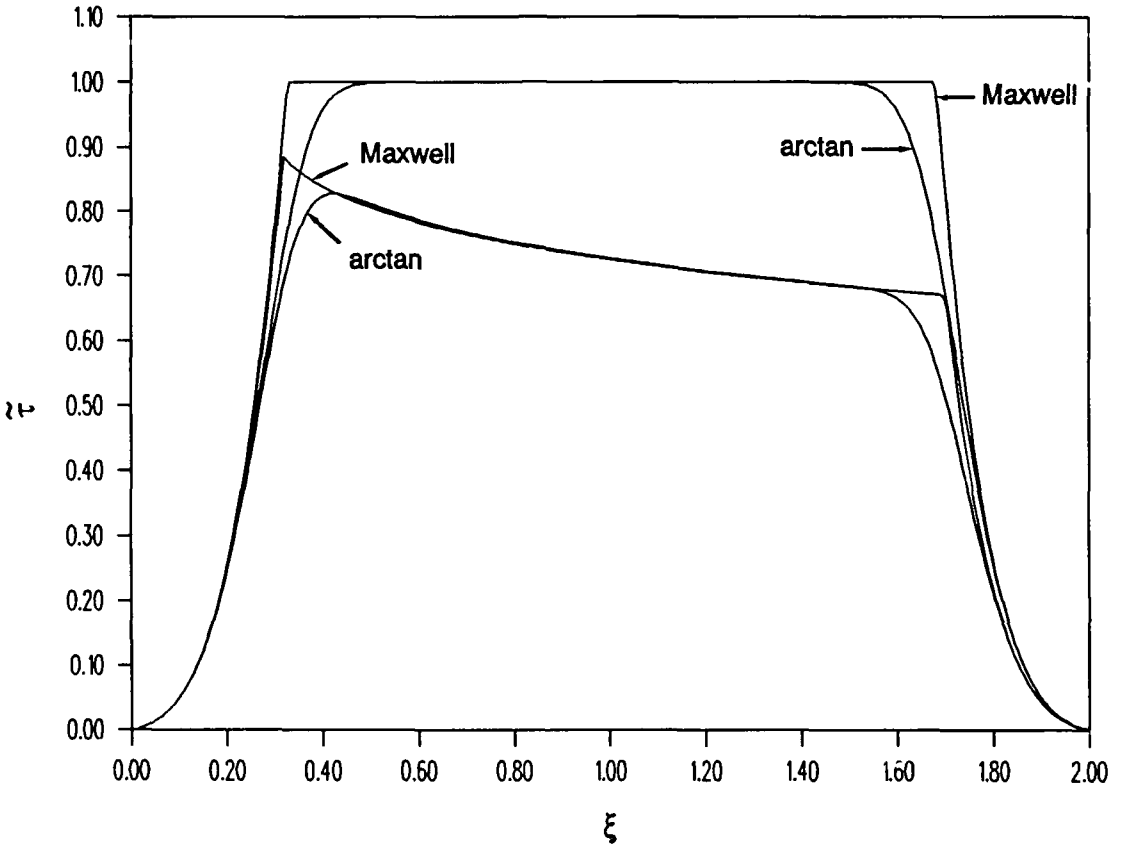

Figure 12. Comparison of shear stress profiles for arctan and Maxwell models; low viscosity, low compliance, s = 0.1 .

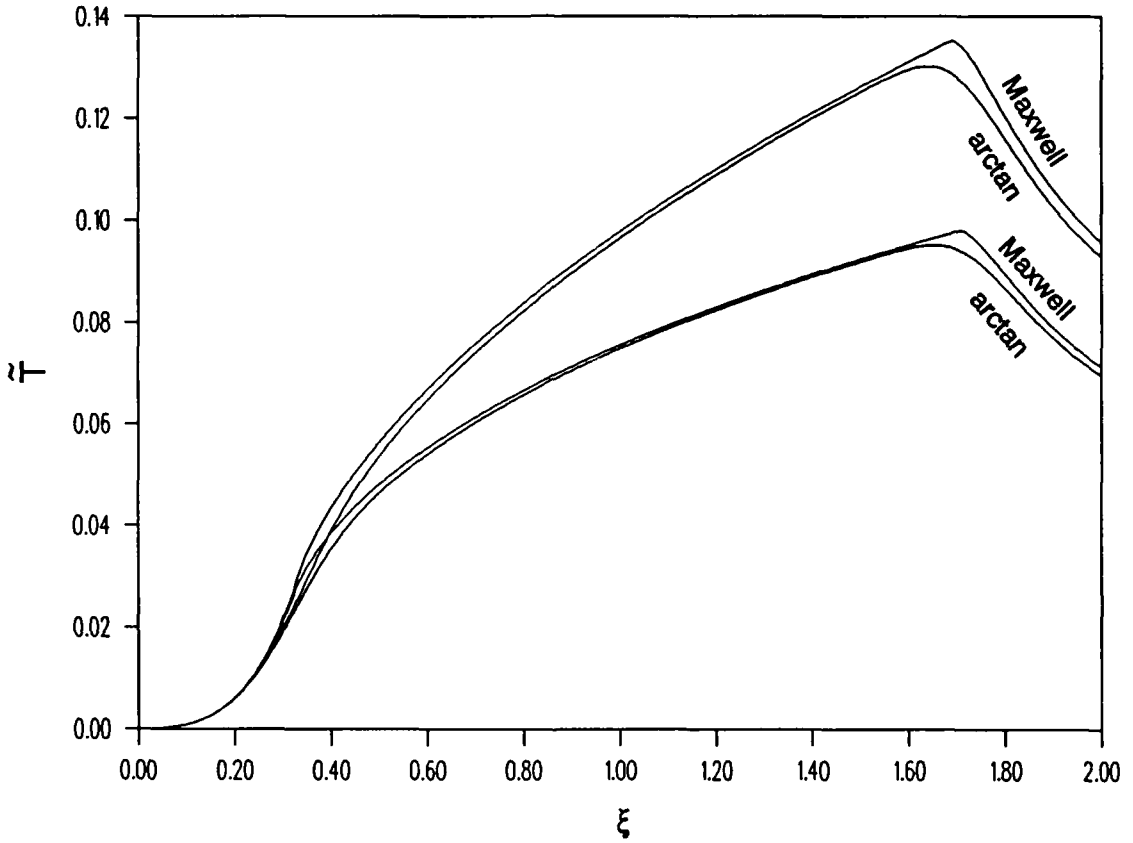

Figure 13. Comparison of dimensionless temperature profiles for arctan and Maxwell models; low viscosity, low compliance, s = 0.1 .

III. TRACTIONS AT HIGH SLIP RATES

The preceding analysis is has been applied to situations where the rolling velocity is high and the slip rates are relatively low. Under these conditions, elasticity effects in the **x** direction can be important and a substantial portion of the shearing can occur below the limiting shear stress. Under conditions of pure sliding or high slide to roll ratios, yielding will occur over the major portion of the contact zone, elastic strains in the film in the **x** direction will be relatively small and visco-plastic deformation will predominate. This can be seen at slide to roll ratios as low as 5% as evidenced by the close proximity of curves (1) and (2) in Figures 2 - 4 under a factor of 10 change in shear modulus. It can further be seen from Figure 4 that at high viscosity the dimensionless average shear stress at a 10% slide to roll ratio falls within 5% of the value of $\bar{\tau} = 1$ which would occur if pure plastic behavior ($\tau = \tau_m$) were to prevail over the entire contact zone.

A. Equations of Plasticity for a Thin Film

The plastic behavior of the lubricant may be analyzed in greater depth than in the previous sections by treating the film as an ideal plastic-rigid material and later generalizing the analysis to include visco-plastic behavior as used previously. The Levy-Von Mises Equations for plane strain deformation of a plastic-rigid material will be presented and then reduced to a thin film form based an a small aspect ratio ($a/h_0 << 1$) analogous to the reduction of the hydrodynamic equations to a lubrication environment.

Development of the Levy-Von Mises Equations can be found in many texts[6,7] and will not be derived here. They consist of equilibrium relationships, stress - strain rate and continuity relationships and a yield criterion. They will be presented here in terms of stresses and instantaneous velocities under conditions of plane strain.

The equilibrium equations are given below:

$$\frac{\partial \sigma_x}{\partial x} + \frac{\partial \tau}{\partial y} = 0 \quad , \tag{17}$$

$$\frac{\partial \tau}{\partial x} + \frac{\partial \sigma_y}{\partial y} = 0 \quad . \tag{18}$$

Equations (17) and (18) represent equilibrium in the **x** and **y** directions respectively.

An effective stress or flow stress, $\bar{\sigma}$, is used in both the stress - strain rate equations and the yield criterion. A corresponding effective strain rate, $\bar{e}$, may also be introduced and expressed in terms of the instantaneous velocities. These are both defined below:

$$\bar{\sigma} = \sqrt{3\left[\left(\frac{\sigma_x - \sigma_y}{2}\right)^2 + \tau^2\right]} \quad , \tag{19}$$

$$\bar{e} = \frac{\sqrt{3}}{2}\sqrt{\left(\frac{\partial u}{\partial x} - \frac{\partial v}{\partial y}\right)^2 + \left(\frac{\partial u}{\partial y} + \frac{\partial v}{\partial x}\right)^2} \quad . \tag{20}$$

The stress - strain rate equations for plane strain may be written in terms of the velocities as follows:

$$\frac{\partial u}{\partial x} = \frac{\bar{e}}{2\bar{\sigma}}(\sigma_x - \sigma_y) \quad , \tag{21}$$

$$\frac{\partial v}{\partial y} = -\frac{\bar{e}}{2\bar{\sigma}}(\sigma_x - \sigma_y) \quad , \tag{22}$$

$$\frac{\partial u}{\partial y} + \frac{\partial v}{\partial x} = \frac{2\bar{e}}{\bar{\sigma}}\tau \quad . \tag{23}$$

The continuity equation may be obtained by adding Equations (21) and (22)

$$\frac{\partial u}{\partial x} + \frac{\partial v}{\partial y} = 0 \quad . \tag{24}$$

Finally the Von Mises yield criterion may be expressed as

$$\bar{\sigma} = \sqrt{3}\,k \quad , \tag{25}$$

where k is the shear yield stress for the coating.

The above equations will now be reduced to a thin film environment by estimating orders of magnitudes for their various terms and neglecting terms of order h_0/a compared with unity. Since the quantities **a** and h_0

represent reasonable scale factors for **x** and **y** in the coating, the dimensionless coordinates ξ and η defined previously will be used here. A characteristic sliding velocity u_0 will be introduced which could be the surface velocity for pure sliding or the slip velocity for a rolling-sliding contact at high slide to roll ratios. This velocity will be used as the scale factor for **u**. An appropriate scale factor reflecting the order of magnitude of **v** would be $u_0 h_0/a$ as can be seen from inspection of the continuity equation. The reduced velocities $\hat{u} = u/u_0$ and $\hat{v} = av/(h_0 u_0)$ will now be introduced and will be assumed, along with the coordinates ξ and η to be of the order of magnitude of **1**. The effective strain rate $\bar{e}$, given in Equation (20) may be written in terms of these variables as

$$\frac{h_0}{u_0}\bar{e} = \frac{\sqrt{3}}{2}\sqrt{\left(\frac{h_0}{a}\right)^2\left(\frac{\partial \hat{u}}{\partial \xi} - \frac{\partial \hat{v}}{\partial \eta}\right)^2 + \left[\frac{\partial \hat{u}}{\partial \eta} + \left(\frac{h_0}{a}\right)^2 \frac{\partial \hat{v}}{\partial \xi}\right]^2} \approx \frac{\sqrt{3}}{2}\frac{\partial \hat{u}}{\partial \eta} \quad . \tag{26}$$

The right hand side of Equation (26) was obtained by neglecting terms of the order of $(h_0/a)^2$ compared with **1**.

One may now substitute the approximate value for $\bar{e}$ obtained from the right hand side of Equation (26) along with the value of $\bar{\sigma}$ given by Equation (25) for the corresponding quantities in Equation (23) and express the result in terms of the reduced variables given above as follows:

$$\frac{\partial \hat{u}}{\partial \eta} + \left(\frac{h_0}{a}\right)^2 \frac{\partial \hat{v}}{\partial \xi} \approx \frac{\partial \hat{u}}{\partial \eta}\frac{\tau}{k} \quad .$$

Again assuming that $\partial \hat{u}/\partial \eta$ is of order **1**, one may neglect the second term on the left side of the above equation and solve the resulting expression for τ to obtain the approximate relationship

$$\tau \approx k \quad , \tag{27}$$

where the departure of τ/k from **1** is of the order of $(h_0/a)^2$. Equation (27) is extremely important in that it requires the coordinate shear stress to be equal to the shear yield stress everywhere in the coating within the contact zone where plastic deformation occurs. Some of the ramifications of this property will be discussed later.

A reference pressure p_0 may be used as a scale for the normal stresses which can be the maximum Hertz

pressure, p_h or any characteristic pressure associated with the normal loading in a non-hertzian contact. One may now introduce the reduced stresses $\hat{\sigma}_x$ and $\hat{\sigma}_y$ in Equation (21) and perform the same substitutions for $\bar{e}$ and $\bar{\sigma}$ as used in deriving Equation (27) above to obtain the approximate relationship

$$(\hat{\sigma}_x - \hat{\sigma}_y)\frac{\partial \hat{u}}{\partial \eta} \sim 4\delta \hat{k}\frac{\partial \hat{u}}{\partial \xi} \quad ,$$

where $\delta = (h_0/a)(k_0/p_0)$, k_0 is the shear yield stress of the coating at ambient pressure and temperature to be used as a characteristic value and $\hat{k} = k/k_0$.

Since the reduced stresses and partial derivatives in the above equation are assumed to be of order 1 and the coefficient on the right hand side is small, the two normal stresses are approximately equal ($\sigma_x \sim \sigma_y$). Furthermore, since for the conditions of plane strain assumed here $\sigma_z = (\sigma_x + \sigma_y)/2$, a nearly hydrostatic state of stress will exist where

$$\sigma_x \sim \sigma_y \sim \sigma_z \sim -p \quad . \tag{28}$$

The relative error in Equation (28) will be of the order of $\delta^* = \max[(h_0/a)^2, \delta]$. All of the arguments presented thus far allow k to be a variable dependent on both temperature and pressure.

One may substitute Equations (27) and (28) for the shear stress and normal stress in Equation (18) to obtain the relationship for the pressure variation across the film

$$\frac{\partial \tilde{p}}{\partial \eta} \sim \delta\frac{\partial \hat{\tau}}{\partial \xi} \sim 0 \quad , \tag{29}$$

where $\hat{\tau} = \tau/k_0 \sim \hat{k}$. The above equation shows the usual result that the pressure does not vary significantly across a thin film along with an indication of the relative error (of the order of δ^*). When the same substitutions are introduced into Equation (17) the following expression is obtained:

$$\frac{\partial \tilde{p}}{\partial \xi} \sim \frac{a}{h_0}\frac{k}{p_0}\frac{\partial \hat{\tau}}{\partial \eta} \quad . \tag{30}$$

Although the coefficient of $\partial\hat{\tau}/\partial\eta$ will be large, $\partial\hat{\tau}/\partial\eta$ itself will be very small. If the shear yield stress were constant then $\hat{k} = 1$ and from Equation (27), $\hat{\tau} = 1 +$ terms of order $(h_0/a)^2$ and the right hand side

of Equation (30) would be of the order of δ. If **k** were to depend on pressure, even to the extent that $\partial\hat{k}/\partial\tilde{p}$ were of order 1, the pressure variation across the film would still be of the order of δ^* and the right hand side of Equation (30) would at the most be of the order of $\max[(k_0/p_0)^2,\delta]$ which will still be small. The above arguments indicate that under ideal plastic conditions the pressure in the contact zone for a thin film under high shear is constant or

$$\frac{\partial\tilde{p}}{\partial\xi} \sim \frac{\partial\tilde{p}}{\partial\eta} \sim 0 \quad . \tag{31}$$

An exception to the above relationship would occur if **k** were strongly dependent on temperature and severe temperature gradients were to exist across the film. It was shown in the first section of this report that such behavior is not likely to occur due to shearing of a thin metallic film.

B. Deformation of an Elastic Substrate Under a Uniform Pressure

The requirement that the pressure must be constant in the contact zone can significantly alter the shape of the contact when elastic substrates are involved. For example, based on plane strain Hertz contact theory, a cylinder of radius r will flattened in the interval $0 < x < 2a$ by an elliptical pressure distribution having an amplitude $p_h = aE/[2r(1-\nu^2)]$. If **d** is taken to be the displacement of the surface of the cylinder relative to a line drawn tangent to the deformed cylinder at the center of contact ($x=a$), then **d** will be zero inside the contact zone and rise sharply outside the contact zone. A dimensionless displacement defined as $\tilde{d} = 2rd/a^2$ is plotted against ξ for both the hertzian pressure distribution described above and for uniform pressures over the interval $0 < x < 2a$ in Figure 14. The curve labeled (a) represents the hertzian displacement. The curve labeled (b) corresponds to the displacement of the same surface under a uniform pressure that integrates to the same load as the hertzian curve (a). The curve labeled (c) is the displacement at the uniform pressure required to flatten the cylinder at the center of contact which may be shown to be twice that used in obtaining curve (b).

Figure 1 depicts a situation where two rollers are loaded together in a hertzian contact and separated by a constant coating thickness in the contact zone. This is generally assumed to occur when the coating thickness is smaller than the overall elastic deformation of the substrates. The shape of the film thickness profile would thus be the same as the sum of the elastic surface displacement profiles. If the sliding rate is sufficiently high to cause a significant degree of yielding, the coating will not support a hertzian pressure profile and the film thickness cannot remain constant. The variations in the substrate surface displacements under a uniform pressure shown in Figure 14 can be large compared with the film thickness thereby

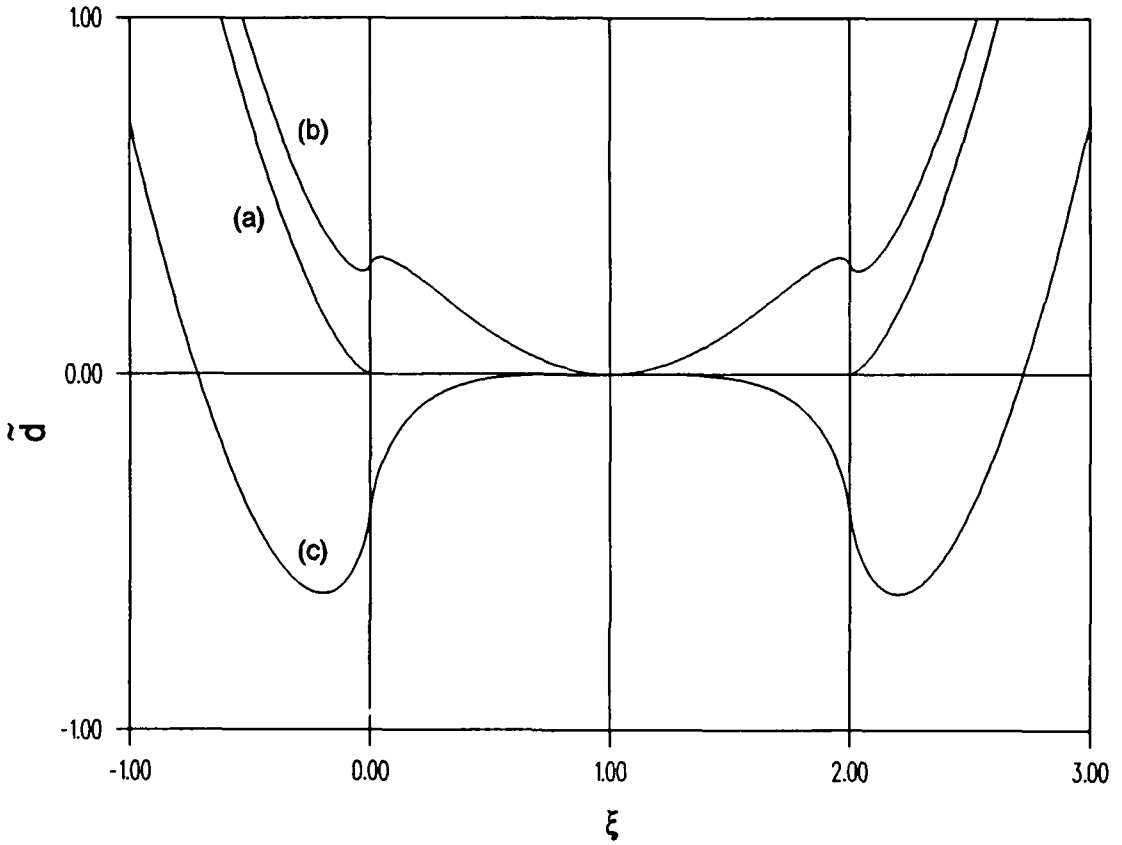

Figure 14. Comparison of dimensionless surface displacement profiles under elliptical and uniform pressure distributions.

producing major film thickness variations.

These film thickness variations have not been treated in the initial traction analysis presented in Section II or in the elastohydrodynamic traction analyses which assume limiting shear behavior due to solidification to occur with a constant film thickness. The above results indicate that substantial qualitative behavioral discrepancies may result from separating the traction theory from the film thickness predictions when solidification or limiting shear behavior is predicted to occur.

C. Example of a Rigid Slider on a Substrate with a Visco-Plastic Coating

Further insight into the effects of plastic yielding at high slip rates may be obtained by considering a visco-plastic film having a rheological model of the form

$$\tau' = \mu \frac{\partial u}{\partial y} , \quad \tau = \min(\tau', k) \quad . \tag{32}$$

A schematic of the film under consideration is shown in Figure 15. If at any point **x**, the shear stress in the film is below the shear yield stress, **k**, then the equilibrium equations for the two dimensional thin film will be given by

$$\frac{\partial p}{\partial x} = \frac{\partial \tau}{\partial y} , \quad \frac{\partial p}{\partial y} = 0 \quad . \tag{33}$$

If the film is assumed to be steady (**w=0 at y=h**), one may integrate the continuity equation given by Equation (28) across the film to obtain the expression

$$\int_0^h u\,dy = Q = \frac{u_0 h^*}{2} \quad , \tag{34}$$

where **Q** denotes the volumetric flow rate per unit transverse length and $h^* = 2Q/u_0$.

Since from Equation (33) the shear stress must vary linearly across the film, it will have its maximum and minimum values at the surfaces. It is thus possible for the shear stress at any given **x** to equal the shear yield stress on one of the surfaces and fall below the shear yield stress and behave in a viscous fashion between the surfaces thereby supporting a pressure gradient along the film. This would be manifested by

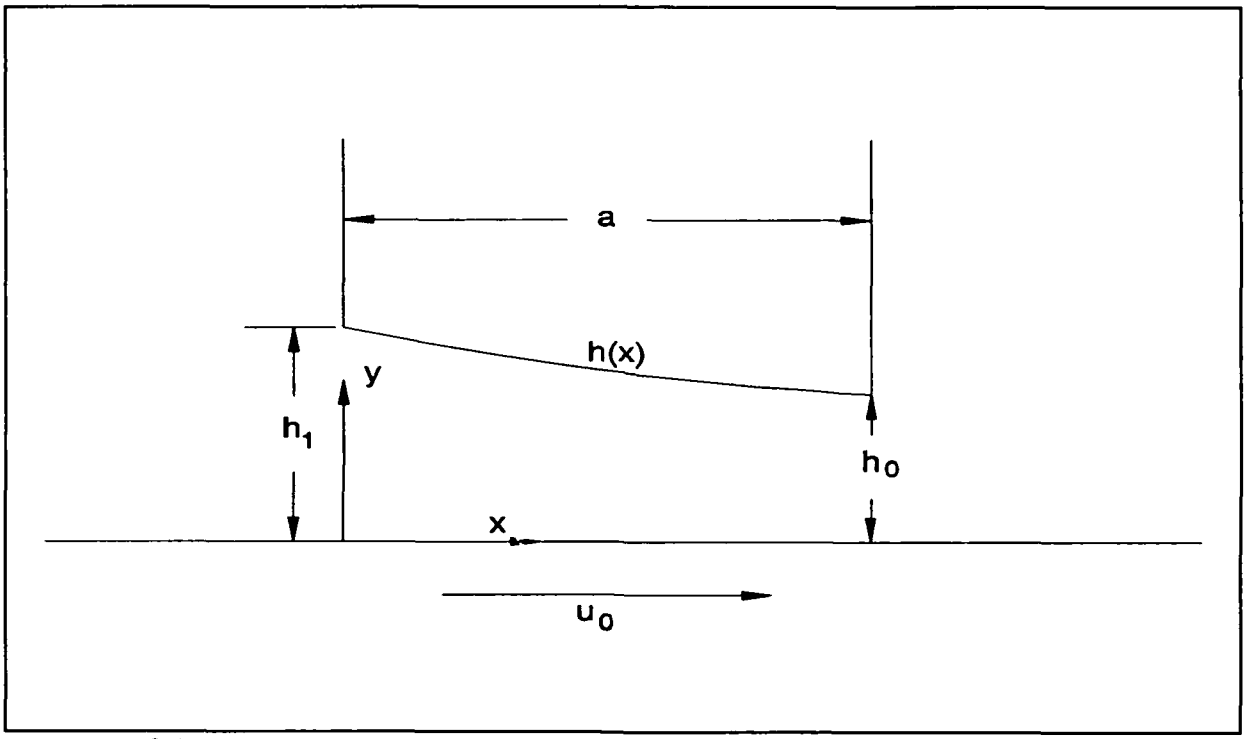

Figure 15. Schematic of variables for slider bearing analysis.

slip at the yield surface. If at any value of **x**, the shear yield is reached at both surfaces (in the same direction) then the shear stress will be constant across the film and from Equation (33) as well as the arguments presented in the preceding section, the pressure gradient along the film must vanish.

For the conditions of pure sliding assumed here, the boundary conditions on the velocity, **u**, under usual conditions of no slip would be $u=u_0$ at $y=0$ and $u=0$ at $y=h$. If slip were to occur at $y=0$ the surface velocity of the coating may be represented as $u_0 - \Delta u_0$ similarly the velocity may be represented as Δu_0 for slip at $y=h$.

One may now differentiate Equation (32) with respect to **y**, substitute Equation(33) for $\partial\tau/\partial y$, integrate the resulting expression subject to the boundary conditions on **u** described above to obtain the velocity distribution

$$u = \frac{1}{2\mu}\frac{\partial p}{\partial x}y(y-h) + (u_0 - \Delta u_0)\frac{(h-y)}{h} + \Delta u_h\frac{y}{h} \quad , \tag{35}$$

which, with the exception of the slip velocities, is part of the procedure generally used in developing the lubrication equations.

The shear stress due to viscous motion may be obtained by differentiating the velocity distribution. The shear stresses at $y=0$, denoted by τ_0 and at $y=h$ by τ_h are given below:

$$-\tau_0 = \mu\frac{u_0}{h} + \frac{h}{2}\frac{\partial p}{\partial x} - \mu\frac{(\Delta u_0 + \Delta u_h)}{h} \quad , \tag{36}$$

$$-\tau_h = \mu\frac{u_0}{h} - \frac{h}{2}\frac{\partial p}{\partial x} - \mu\frac{(\Delta u_0 + \Delta u_h)}{h} \quad . \tag{37}$$

One may substitute Equation (35) for u in Equation (34) and integrate the resulting equation across the film to obtain the flow relationship

$$\frac{h^3}{12\mu}\frac{\partial p}{\partial x} = \frac{u_0}{2}(h - h^*) + \frac{\Delta u_h - \Delta u_0}{2}h \quad . \tag{38}$$

For the example here of pure sliding with a monatonically decreasing film thickness, four modes of shearing

will exist depending on the values of the surface shear stresses $-\tau_0$ and $-\tau_h$ in relation to the shear yield stress **k**. (It should be noted that the minus signs are used here since an absolute value is required for comparing the shear stress to the shear yield stress and for the coordinate system in this example with the surface at **y=0** in motion, the shear stresses will in general be negative when their magnitudes approach the yield value.) These will be described below.

Case 1. No slip, $-\tau_0$, $-\tau_h < k$. The motion in this case will be purely viscous with $\Delta u_0 = \Delta u_h = 0$ and Equation (38) reduces to

$$\frac{\partial p}{\partial x} = 6\mu u_0 \frac{(h - h^*)}{h^3} \quad .$$

Case 2. Slip at y=0, no slip at y=h, $-\tau_0 = k$, $-\tau_h < k$. One may set $-\tau_0 = k$ and $\Delta u_h = 0$ in Equation (36) and solve for Δu_0 to obtain relationship

$$\Delta u_0 = u_0 + \frac{h^2}{2\mu}\frac{\partial p}{\partial x} - \frac{kh}{\mu} \quad ,$$

which may be substituted for Δu_0 in Equation (38) which is in turn solved for the pressure gradient

$$\frac{\partial p}{\partial x} = \frac{3\mu u_0}{2h^3}\left(\frac{kh^2}{\mu u_0} - h^*\right) \quad .$$

Case 3. Slip at y=h, no slip at y=0, $-\tau_h = k$, $-\tau_0 < k$. One may set $-\tau_h = k$ and $\Delta u_0 = 0$ in Equation (37) which maybe solved for Δu_h and combined with Equation (38) as in Case 2 to obtain the following relationships for the slip velocity and the pressure gradient:

$$\Delta u_h = u_0 - \frac{h^2}{2\mu}\frac{\partial p}{\partial x} - \frac{kh}{\mu} \quad ,$$

$$\frac{\partial p}{\partial x} = \frac{3\mu u_0}{2h^3}\left(2h - h^* - \frac{kh^2}{\mu u_0}\right) \quad .$$

Case 4. Slip at y=0 and y=h, $-\tau_0 = k$, $-\tau_h = k$. Here the interior of the film will be plastic hence the pressure gradient must vanish

$$\frac{\partial p}{\partial x} = 0 \quad .$$

The relationships for the pressure gradients and surface shear stresses for the various cases may be put in dimensionless form with the use of the following additional dimensionless variables and parameters

$$\hat{\tau}_0 = -\frac{\tau_0}{k}, \quad \hat{\tau}_h = -\frac{\tau_h}{k}, \quad \hat{p} = \frac{h_0}{ak} p, \quad \hat{h} = \frac{h}{h_0}, \quad \hat{h}_1 = \frac{h_1}{h_0}, \quad \hat{h}^* = \frac{h^*}{h_0}, \quad \hat{\mu} = \frac{\mu u_0}{h_0 k} .$$

The results are summarized below:

$$\frac{\partial \hat{p}}{\partial \xi} = \begin{cases} 6\hat{\mu}\dfrac{\hat{h} - \hat{h}^*}{\hat{h}^3} & , \text{Case 1} \\ \dfrac{3}{2}\dfrac{\hat{h}^2 - \hat{h}^*\hat{\mu}}{\hat{h}^3} & , \text{Case 2} \\ \dfrac{3}{2}\dfrac{2\hat{\mu}\hat{h} - \hat{h}^2 - \hat{\mu}\hat{h}^*}{\hat{h}^3} & , \text{Case 3} \\ 0 & , \text{Case 4} \end{cases} , \tag{39}$$

$$\hat{\tau}_0 = \begin{cases} \dfrac{\hat{\mu}}{\hat{h}} + \dfrac{\hat{h}}{2}\dfrac{\partial \hat{p}}{\partial \xi} & , \text{Case 1} \\ 1 & , \text{Case 2} \\ 1 + \hat{h}\dfrac{\partial \hat{p}}{\partial \xi} & , \text{Case 3} \\ 1 & , \text{Case 4} \end{cases} , \tag{40}$$

$$\hat{\tau}_h = \begin{cases} \dfrac{\hat{\mu}}{\hat{h}} - \dfrac{\hat{h}}{2}\dfrac{\partial \hat{p}}{\partial \xi} & , \text{Case 1} \\ 1 - \hat{h}\dfrac{\partial \hat{p}}{\partial \xi} & , \text{Case 2} \\ 1 & , \text{Case 3} \\ 1 & , \text{Case 4} \end{cases} . \tag{41}$$

The above equations provide an analytical procedure for determining the pressure gradient and surface shear stress which is combined with a numerical procedure for determining the value of h^* required to satisfy the boundary conditions on the pressure that $\hat{p} = 0$ at $\xi = 0,1$ which may be expressed mathematically by integrating Equation (39)

$$\int_0^1 \frac{\partial \hat{p}}{\partial \xi} d\xi - 0 \quad . \tag{42}$$

The solution algorithm first involves dividing the interval $0 \leq \xi \leq 1$ into a discreet number of points and selecting a trial value of $\hat{h}^*$. Starting at the first point one may now compute the pressure gradient and corresponding surface shear stresses using the Case 1 form of Equations (39) - (41) denoting the maximum of $\hat{\tau}_0$ and $\hat{\tau}_h$ as $\hat{\tau}_{max}$ for Case 1. If $\hat{\tau}_{max} \leq 1$, one may save the value of the pressure gradient and proceed to the next point. If for Case 1, $\hat{\tau}_{max} > 1$ and $\partial\hat{p}/\partial\xi > 0$, the solution will either correspond to Case 2 or Case 4. To determine which, compute the pressure gradient and shear stresses for Case 2. If $\hat{\tau}_h \leq 1$ proceed to the next point. If not, set the pressure gradient and shear stresses to their Case 4 values and proceed to the next point. If for Case 1 $\hat{\tau}_{max} > 1$ and $\partial\hat{p}/\partial\xi < 0$ the solution will either correspond to Case 3 or Case 4. To determine which, compute the pressure gradient and shear stresses for Case 3. If $\hat{\tau}_0 \leq 1$ proceed to the next point. If not, set the pressure gradient and shear stresses to their Case 4 values and proceed to the next point.

The above procedure may be used to determine the pressure gradient at every point which may then be used for numerical integration of the left side Equation (42). The correct value of $\hat{h}^*$ will be the one that satisfies Equation (42). For the present analysis, numerical integration was carried out using the trapezoidal rule and $\hat{h}^*$ was determined using the Brent method[3]. The combined analytical and numerical procedure used here is a reduction of a general purpose numerical algorithm developed by the author for treating classes of one dimensional non-newtonian rolling-sliding contacts in powder lubrication[8].

Once the pressure gradients are determined they may be integrated with respect to ξ to compute the pressure distribution which may in turn be integrated to predict the dimensionless load $\hat{W}$. One may also integrate $\hat{\tau}_0$ given by Equation (40) to compute the tractive force. These dimensionless forces are defined as

$$\hat{W} = \frac{h_0}{a^2 k} W = \int_0^1 \hat{p}\, d\xi \,, \quad \hat{f} = \frac{f}{ak} = \int_0^1 \hat{\tau}_0\, d\xi \,,$$

where **W** and **f** denote normal and frictional forces per unit transverse length.

Computations have been carried out for the case of a convergent slider with a linear film thickness profile given by

$$\hat{h} = \hat{h}_1 - (\hat{h}_1 - 1)\xi \,, \quad 0 \le \xi \le 1 \quad .$$

The variation of the dimensionless load capacity, $\hat{W}$ and traction, $\hat{f}$, with the viscosity-speed parameter $\hat{\mu}$, are given in Figures 16 and 17 respectively at various values of the film thickness ratio $\hat{h}_1$. The parameter $\hat{\mu}$ is an index of the relative magnitude of the viscous shear force to the yield stress and is proportional to both the viscosity and the sliding speed. At low values of $\hat{\mu}$ the flow will be entirely viscous in nature with shear stresses below the yield stress everywhere in the film. At the points denoted by the small dots (·) in Figure 16, the shear yield stress is reached on the stationary surface at the trailing edge where the film thickness is smallest. As $\hat{\mu}$ is increased further the general level of shear goes up in the film and the zone at which trailing edge slip occurs increases. At the points denoted by the circles (◦) the shear yield stress is reached and slip starts to occur on the moving surface near the leading edge of the film. As $\hat{\mu}$ continues to increase, both slip zones expand inward until they eventually overlap. Points of incipient overlap are indicated by the intersections of the various curves with the broken line in Figure 16.

The behavior of the film at values of $\hat{\mu}$ to the right of the broken line can be observed by examining the pressure profiles shown in Figure 18 for the particular case of $\hat{h}_1 = 3$. The top curve corresponds to the threshold value of $\hat{\mu}$ where yield across the film occurs at one point. As $\hat{\mu}$ increases the fully plastic zone, as manifested by the flat portions of the curves, expand and the pressures drop. As the sliding speed (or viscosity) becomes high enough the plastic zone extends to the entire film and the pressure (hence the load capacity) falls to **0**. As can be seen from Figure 16, this complete loss of load capacity occurs at finite defined values of $\hat{\mu}$ which depend only on the film thickness ratio. This value of $\hat{\mu}$ which will be denoted by $\hat{\mu}^*$ may be computed from Equation (39) for any smoothly convergent film as shown below.

Just before the entire film becomes plastic a small region will exist in the inlet where Case 2 shear prevails and a region at the exit where Case 3 shear prevails. The pressure gradient must approach 0 as each of these regions merge with the fully plastic region. As the length of the Case 2 inlet region becomes very

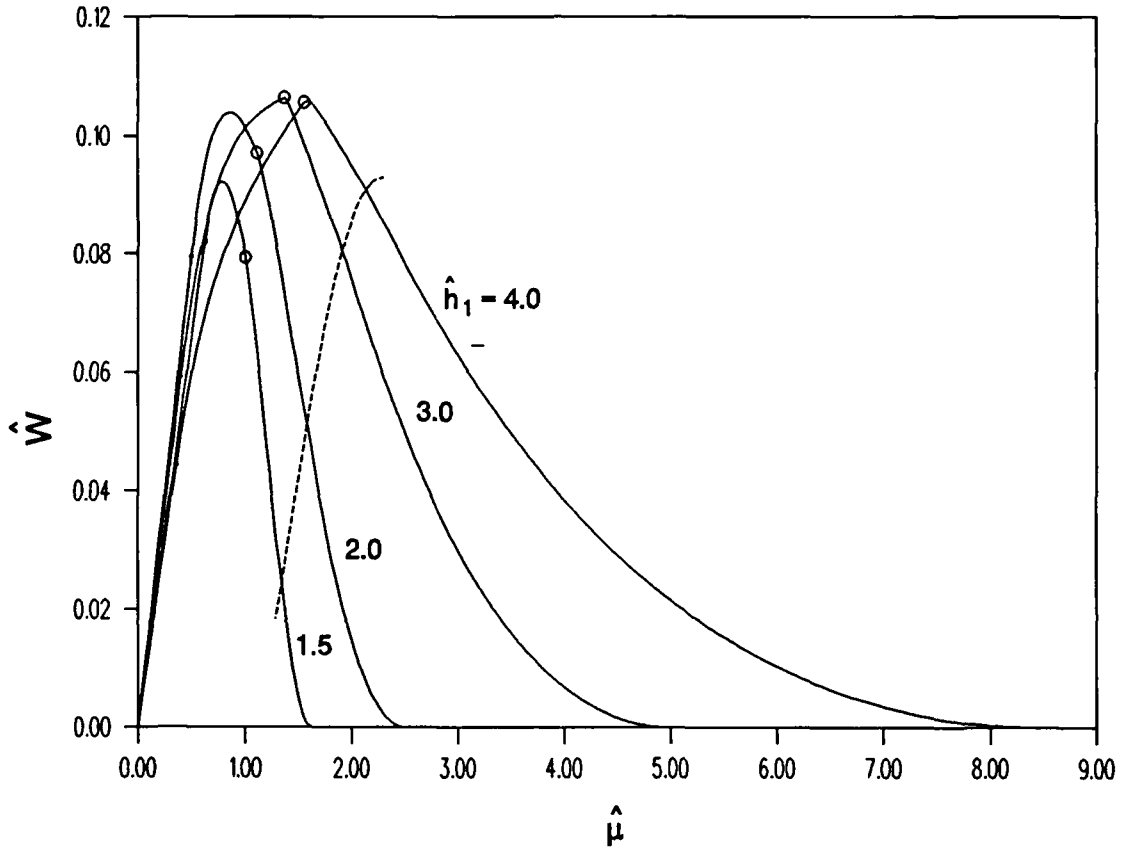

Figure 16. The variation of dimensionless load capacity with viscosity - speed parameter for a linear slider bearing.

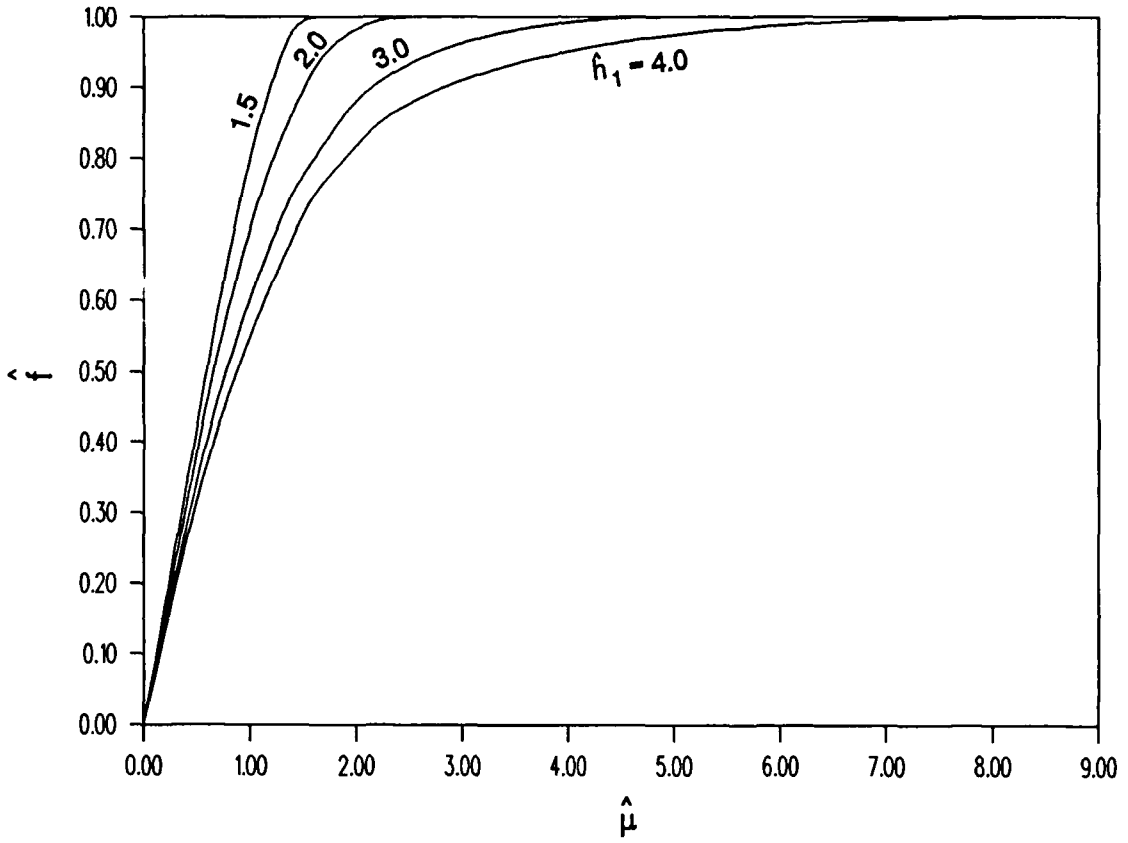

Figure 17. The variation of dimensionless traction with viscosity - speed parameter for a linear slider bearing.

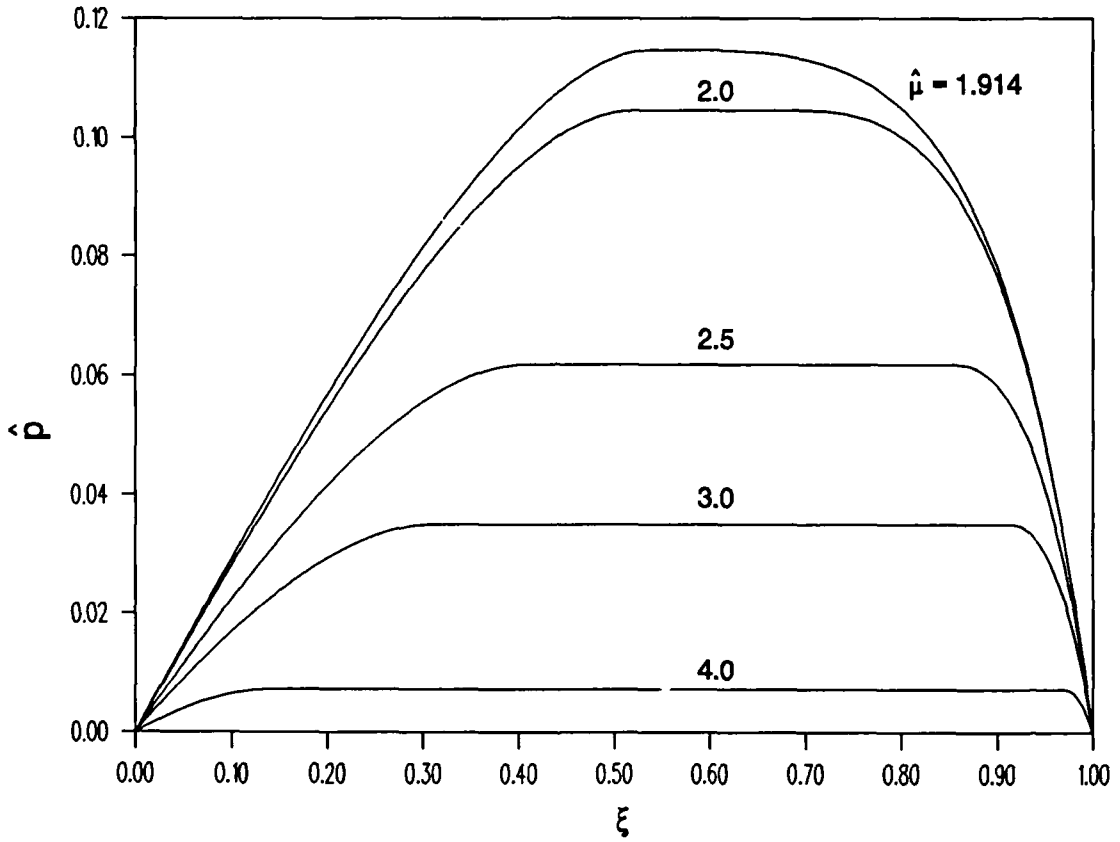

Figure 18. The variation of $\hat{p}$ with $\hat{\xi}$, at various values of μ, for a linear slider with $\hat{h}_1 = 3$.

small the film thickness $\hat{h}$ will approach $\hat{h}_1$. By replacing $\hat{\mu}$ with $\hat{\mu}_m$, $\hat{h}$ with $\hat{h}_1$, and setting the pressure gradient to **0** for Case 2 of Equation (39) one obtains the relationship

$$\hat{h}^*\hat{\mu}_m - \hat{h}_1^2 \quad . \tag{43}$$

One may apply a similar argument to the exit region and replace $\hat{\mu}$ with $\hat{\mu}_m$, $\hat{h}$ with **1**, and set the pressure gradient to **0** for Case 3 of Equation (39), then use Equation (43) to eliminate $\hat{h}^*$ and solve the resulting expression for $\hat{\mu}^*$

$$\hat{\mu}^* - \frac{1 + \hat{h}_1^2}{2} \quad . \tag{44}$$

Thus for any given inclination, $\Delta h = h_1 - h_0$ and minimum film thickness h_0, the load capacity will vanish when the product of the viscosity and sliding speed become high enough so that $\hat{\mu} \geq \hat{\mu}^*$. The variation of film thickness with speed or viscosity at fixed load and inclination can be obtained by plotting the variation of $h_0/\Delta h = 1/(\hat{h}_1\text{-}1)$ with $\mu u_0/(k\Delta h) = \hat{\mu}/(\hat{h}_1\text{-}1)$ at fixed values of $W\Delta h/(a^2k) = \hat{W}(\hat{h}_1\text{-}1)$. This may be obtained from cross plots of the type of data used in generating Figure 16 and is shown for the particular case of $\hat{W}(\hat{h}_1\text{-}1) = .04$, in Figure 19.

The film thickness as shown by solid curve in Figure 19 is seen to increase with increasing speed (or viscosity) at low speeds then reach a maximum and fall off suddenly as plastic yielding starts to occur. The minimum film thickness then continues to decrease but at a less drastic rate. The ratio of the inclination of the trailing edge film thickness at the right end of the solid curve is 16 to 1 which is essentially an edge loading condition. In a separate computation stiffnesses were calculated and found to be negative for the portion of the solid curve having a positive slope and lying to the right of the maximum, indicating an unstable region. In a transient analysis one would expect a rapid drop in film thickness in this region at a rate controlled by squeeze film effects. The dashed line in the figure indicates the film thickness vs. speed behavior that would be predicted to occur in the absence of plastic yielding and demonstrates the drastic effect that plastic yielding is predicted to have on film thickness at high viscosity or speed.

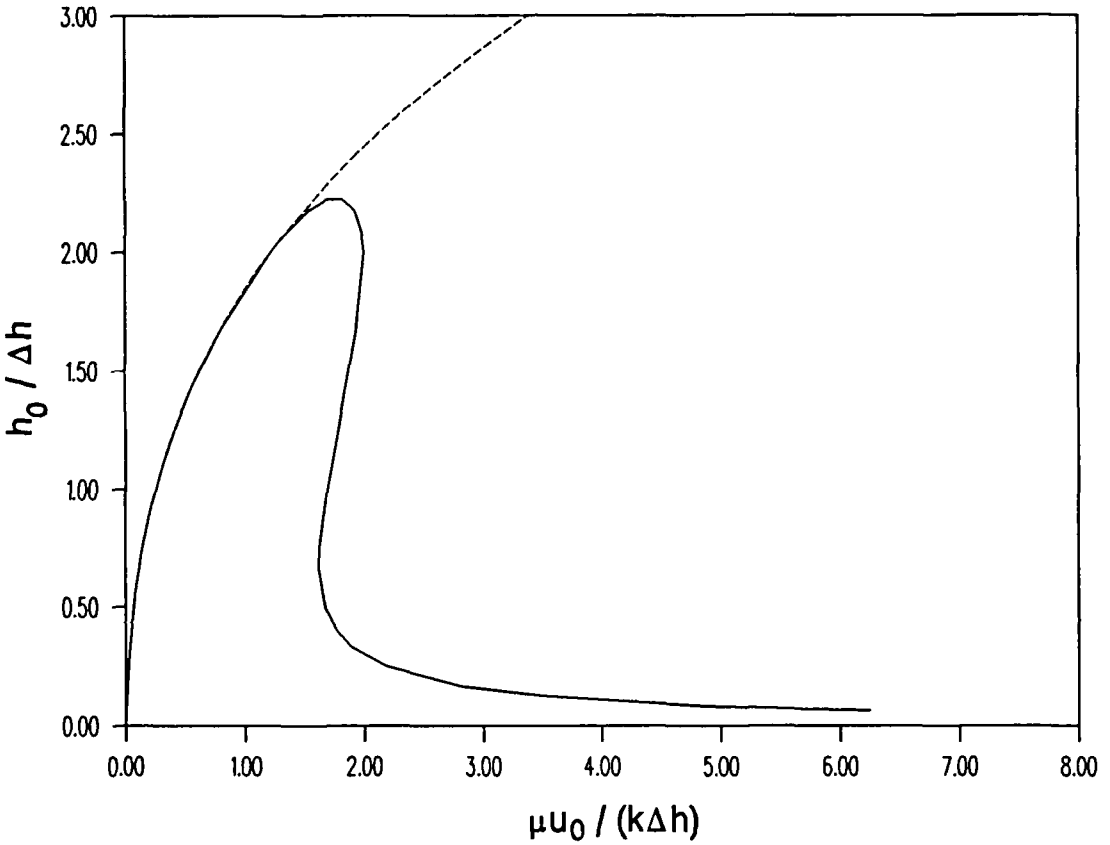

Figure 19. Dimensionless variation of film thickness with speed or viscosity at fixed load and inclination.

IV. SUMMARY AND CONCLUSIONS

Analyses are developed to predict the tractive forces that will occur in a rolling-sliding contact between one body of a single material and a second substrate having a thin coating of solid lubricant. The materials are assumed to be isotropic and conditions of plane strain are assumed to prevail. The film is taken to be thick compared with asperity heights but very thin compared with contact lengths. The coating is assumed to be soft compared with the substrates and the contact pressures are assumed to be high compared with the shear yield stress of the coating.

An initial traction analysis is given in Section II which includes elastic, plastic, creep and thermal effects. The analysis was designed to treat rolling dominated rolling-sliding contacts and incorporates an approach developed for treating solidification in elasto-hydrodynamic contacts but oriented toward the characteristics of solid films with the inclusion of a suitable thermal model. Parametric studies have been performed showing the interaction of the various effects for two rheological models. The analysis has additional flexibility that has not yet been exploited such as capability of handling more general thermal boundary conditions, inclusion of non-hertzian pressure profiles and other rheological models. It is also highly tractable and has the capability being extended to handle real three dimensional contacts with variable slip rate etc., characteristic of real machinery.

An analysis was formulated for a coating under sliding dominated conditions in Section III. Elasticity effects for the coating were neglected and the Levy-Von Mises Equations for a plastic-rigid system were reduced based on thin film approximations. The analysis shows that the coating will both be in a hydrostatic state of stress and will not in general, be able to support a pressure gradient once yielding occurs. This latter result imposes serious restrictions on the assumption of a constant film thickness used in Section I, as well as References 1 and 2 and related elastohydrodynamic traction analyses that use limiting shear theory, at high slip rates.

A simple viscoplastic model was applied to a coating on a rigid substrate moving under a converging rigid slider which permitted yielding within the film or at the coating-substrate interfaces together with viscous motion of the coating at stress levels below the yield point. When yielding occurred at both surfaces at any given location then the film would be at a completely plastic state at that location hence unable to support a pressure gradient. The results show that for any given lubricant, inclination and minimum film thickness there is a critical speed that when exceeded results in a complete loss of load capacity. At a fixed load and inclination, the film thickness is shown to drop off rapidly as significant yielding occurs resulting in extremely small film thicknesses compared with those predicted in the absence of yielding.

In the case of hertzian contact, if the viscosity is highly pressure dependent as assumed in Section II and the shear rates are sufficiently low so that yielding occurs over a relatively small portion of the contact zone, near hertzian pressures (exception for a small amount of flattening near the center of contact) hence a relatively constant film thickness in the contact zone can be maintained. As the shear rate becomes sufficiency high to cause yielding to occur over a major portion of the contact zone a large constant pressure region will develop and sharp variations in the film will occur in the case of compliant substrates of thin films which make it inappropriate to separate traction and film thickness theories.

V. RECOMMENDATIONS

The conclusions of the work performed thus far indicate that it is possible to predict tractions including elastic, plastic, creep and thermal interactions under suitable conditions but more work is needed to extend the results further into the plastic regime. In particular a combined film thickness and traction theory is needed to extend the present analysis as well as previous elastohydrodynamic analyses to account for the effects of lubricant plasticity on the film thickness profile.

While the results of this study indicate the feasibility of a continuum approach to certain modes of solid lubrication, the scope needs to be enlarged to treat non-isotropic lubricants such as MoS_2, as well as three dimensional and transient contacts characteristic of real machinery.

Predictions of small film thicknesses do not necessarily imply failure of the solid lubricant. When the local coating thickness is of the same order of magnitude or smaller than asperity heights on the substrate, they will interact both with the coating and with each other. These interactions need to be considered in conjunction with the lubricant model to provide a general theory that bridges the gap between thick films and classical friction theory.

Experimental verification is badly needed both regarding the predicted variations in film thickness at high slip rates and the range of validity assumptions used in developing the initial traction model in Section II. It will also provide guidance for treating the recommended theoretical extensions. In addition, the various lubricant models require property data which may be extracted from experiments under laboratory conditions simulating actual contacts when primary laboratory data are not readily obtainable.

VI. LITERATURE CITED

1. Bair, S. and Winer, W.O., *"A Rheological Model for Elastohydrodynamic Contacts Based on Primary Laboratory Data"*, ASME J. Lub. Tech., V101, 3, (1979), pp.258-265

2. Tevaarwerk, J.L. and Johnson, K.L., *"The Influence of Fluid Rheology on the Performance of Traction Drives"*, ASME J. Lub. Tech., V101, 3, (1979), pp.266-274

3. Carslaw, H.S. and Jaeger, J.C., *"Conduction of Heat in Solids"*, Oxford University Press, (1959)

4. Press, W.H., Flannery, B.P., Teukolsky, S.A. and Vetterling, W.T., *"Numerical Recipes"*, Cambridge University Press, (1986)

5. Gupta, P.K., and Walowit, J.A., *"Modeling of Stresses in Coated Solids - Phase I"*, WRDC-TR-90- , April, (1990)

6. Thomsen, E.G., Yang, C.T. and Kobayashi, S., *"Mechanics of Plastic Deformation in Metal Processing"*, Macmillan, (1965)

7. Walowit, J.A. and Anno, J.N., *"Modern Developments in Lubrication Mechanics"*, Elsevier, (1975)

8. Heshmat, H., *"Powder-Lubricated Piston Ring Development"*, MTI 89TR28, Prepared for U.S. Army Aviation R&T, NASA LeRC, June, (1989)